Reaction mechanism and pathway for the selective photocatalytic hydrogenation of

nitroaromatics over TiO$_2$ in alcohols

Miss Pimchanok Nakchuai

จุฬาลงกรณ์มหาวิทยาลัย

CHULALONGKORN UNIVERSITY

A Thesis Submitted in Partial Fulfillment of the Requirements

for the Degree of Master of Engineering in Chemical Engineering

Department of Chemical Engineering

Faculty of Engineering

Chulalongkorn University

Academic Year 2018

กลไกและขั้นตอนการเกิดปฏิกิริยาไฮโดรจีเนชั่นแบบเลือกเกิดโดยใช้แสงของไนโตรอะโรมาติก บน
ไทเทเนียมไดออกไซด์ในแอลกอฮอล์

น.ส.พิมพ์ชนก นาคช่วย

วิทยานิพนธ์นี้เป็นส่วนหนึ่งของการศึกษาตามหลักสูตรปริญญาวิศวกรรมศาสตรมหาบัณฑิต
สาขาวิชาวิศวกรรมเคมี ภาควิชาวิศวกรรมเคมี
คณะวิศวกรรมศาสตร์ จุฬาลงกรณ์มหาวิทยาลัย
ปีการศึกษา 2561

Thesis Title	Reaction mechanism and pathway for the selective photocatalytic hydrogenation of nitroaromatics over TiO_2 in alcohols
By	Miss Pimchanok Nakchuai
Field of Study	Chemical Engineering
Thesis Advisor	Professor PIYASAN PRASERTHDAM, Dr.Ing.

Accepted by the Faculty of Engineering, Chulalongkorn University in Partial Fulfillment of the Requirement for the Master of Engineering

.... Dean of the Faculty of Engineering

(Professor SUPOT TEACHAVORASINSKUN, D.Eng.)

THESIS COMMITTEE

.... Chairman

(Professor MUENDUEN PHISALAPHONG, Ph.D.)

.... Thesis Advisor

(Professor PIYASAN PRASERTHDAM, Dr.Ing.)

.... Examiner

(Pongtorn Charoensuppanimit, Ph.D.)

.... External Examiner

(Assistant Professor Okorn Mekasuwandumrong, D.Eng.)

พิมพ์ชนก นาคช่วย : กลไกและขั้นตอนการเกิดปฏิกิริยาไฮโดรจีเนชั่นแบบเลือกเกิด
โดยใช้แสงของไนโตรอะโรมาติก บนไทเทเนียมไดออกไซด์ในแอลกอฮอล์. (Reaction
mechanism and pathway for the selective photocatalytic hydrogenation of
nitroaromatics over TiO$_2$ in alcohols) อ.ที่ปรึกษาหลัก : ศ. ดร.ปิยะสาร ประเสริฐ
ธรรม

งานวิจัยนี้ศึกษากลไกและประสิทธิภาพการเกิดปฏิกิริยาไฮโดรจีเนชั่นแบบเลือกเกิด
โดยใช้แสงของไนโตรอะโรมาติกชนิดต่างกันในตัวทำละลายแอลกอฮอล์หลายชนิดภายใต้การ
การฉายแสงยูวีบนไทเทเนียมไดออกไซด์ที่อุณหภูมิห้องและความดันบรรยากาศ นอกจากนี้ยัง
ศึกษาผลของแพลทินัมบนตัวรองรับไทเทเนียมไดออกไซด์ต่อการเกิดปฏิกิริยา ไนโตรอะโรมาติก
จะถูกเปลี่ยนเป็นอะมิโนอะโรมาติกที่มีค่าการเปลี่ยนแปลงไนโตรอะโรมาติกและค่าการเลือก
เกิดอะมิโนอะโรมาติกสูงเกือบ 100 เปอร์เซ็นต์ ปริมาณการเกิดอะมิโนอะโรมาติกกับ
สารประกอบคาร์บอนิลเป็นไปตามสัดส่วนประมาณ 1:3 อะเซตัลดีไฮด์ อะซิโตนและบิวทาโนน
ถูกผลิตได้จากปฏิกิริยาออกซิเดชั่นของเอทานอล 2-โพรพานอลและบิวทานอล ตามลำดับ เอทา
นอลทำให้ไนโตรอะโรมาติกเปลี่ยนแปลงเร็วที่สุดสิ้นสุดที่ 2 ชั่วโมงเนื่องจากเอทานอลผลิต
ไฮโดรเจนไอออนได้ประสิทธิภาพที่สุด นอกจากนี้ แพลทินัมบนตัวรองรับไทเทเนียมไดออกไซด์
ให้ประสิทธิภาพการเกิดปฏิกิริยาสูงกว่าตัวรองรับไทเทเนียมไดออกไซด์ สอดคล้องกับผลการ
วิเคราะห์ด้วยเทคนิคยูวี-วิสิเบิลสเปกโทรสโคปี เอ็กซเรย์โฟโตอิเล็กตรอนสเปกโทรสโคปี และโฟ
โตลูมิเนสเซ้นส์สเปกโทรมิเตอร์ ซึ่งแพลทินัมบนตัวรองรับไทเทเนียมไดออกไซด์ส่งเสริมการถ่าย
โอนอิเล็กตรอนและชะลอการกลับมารวมกันของคู่อิเล็กตรอนและโฮล ดังนั้น ประสิทธิภาพการ
เกิดปฏิกิริยาเป็นผลมาจากตัวให้ไฮโดรเจนและประสิทธิภาพในการแยกคู่ประจุของตัวเร่ง
ปฏิกิริยา จากการเปลี่ยนชนิดสารตั้งต้น ความเข้มข้นของสารตั้งต้น ชนิดตัวทำละลาย
แอลกอฮอล์ และตัวเร่งปฏิกิริยา ชี้ให้เห็นว่าประสิทธิภาพการเกิดปฏิกิริยาไฮโดรจีเนชั่นแบบ
เลือกเกิดโดยใช้แสงของไนโตรอะโรมาติกไม่ได้ขึ้นอยู่กับสารตั้งต้นแต่ขึ้นอยู่กับอัตราการเกิด
ไฮโดรเจนไอออนจากปฏิกิริยาออกซิเดชั่นของแอลกอฮอล์ด้วยโฮล

สาขาวิชา	วิศวกรรมเคมี	ลายมือชื่อนิสิต
		....
ปี	2561	ลายมือชื่อ อ.ที่ปรึกษาหลัก
การศึกษา		....

6070261621 : MAJOR CHEMICAL ENGINEERING

KEYWORD: Photocatalytic hydrogenation; Nitroaromatics; Titanium dioxide

Pimchanok Nakchuai : Reaction mechanism and pathway for the selective photocatalytic hydrogenation of nitroaromatics over TiO_2 in alcohols. Advisor: Prof. PIYASAN PRASERTHDAM, Dr.Ing.

This research investigated the mechanism and photocatalytic performance of the selective photocatalytic hydrogenation of different nitroaromatics ($Ar-NO_2$) in several alcohols under UV light using $P25-TiO_2$ at room temperature and atmospheric pressure. The effect of Pt-deposited $P25-TiO_2$ on the photocatalytic performance was also studied. $Ar-NO_2$ was converted to aminoaromatics ($Ar-NH_2$) with high $Ar-NO_2$ conversion and $Ar-NH_2$ selectivity at nearly 100%. The amounts of $Ar-NH_2$ were proportional with carbonyl compounds at the ratio around 1:3. Acetaldehyde, acetone, and butanone were produced by oxidation of ethanol, 2-propanol, and butanol, respectively. Ethanol exhibited the fastest completed $Ar-NO_2$ conversion due to the most efficient formation of hydrogen ions (H^+). Moreover, Pt/P25 exhibited higher photocatalytic activity than $P25-TiO_2$, which was in good agreement with the UV-Vis, XPS, and PL results. Pt/P25 promoted electron transfer and retard electron-hole recombination. Accordingly, the photocatalytic activity was influenced by hydrogen donor and charge separation efficiency of the catalyst. From varying the substrate, the concentration of substrate, alcoholic solvents, and the catalyst, this suggested that the photocatalytic performance of this reaction did not rely on the substrate but depended on H^+ formation rate from the oxidation of alcohol by hole (h^+).

Field of Study:	Chemical Engineering	Student's Signature
		....
Academic Year:	2018	Advisor's Signature
		....

ACKNOWLEDGEMENTS

This thesis would not have been completed without the support from the following individuals.

Firstly, I offer my gratitude to my thesis advisor, Professor Dr. Piyasan Praserthdam for his supervision, valuable advice and guidance since the very early stage of this research as well as giving me extraordinary experiences throughout the work.

Secondly, I would like to acknowledge Professor Dr. Muenduen Phisalaphong of the Department of Chemical Engineering at Chulalongkorn University, as my thesis chairman, Dr. Pongtorn Charoensuppanimit of the Department of Chemical Engineering at Chulalongkorn University, and Assistant Professor Dr. Okorn Mekasuwandumrong of the Department of Chemical Engineering at Silpakorn University, as my thesis committee and examiner.

Thirdly, I would like to thank my friends and the scientists at the Center of Excellence in Catalysis and Catalytic Reaction Engineering, who always give assistance and encouragement throughout this thesis.

Finally, I gratefully thank my family for their encouragements and supports throughout my study and the period of this thesis.

Pimchanok Nakchuai

TABLE OF CONTENTS

จุฬาลงกรณ์มหาวิทยาลัย
CHULALONGKORN UNIVERSITY

LIST OF TABLES

LIST OF FIGURES

CHAPTER 1

INTRODUCTION

1.1 Introduction

Functionalized anilines or aminoaromatics (Ar-NH$_2$) are organic molecules that are important intermediates for the synthesis of fine chemicals, pharmaceutical, polymers, pigments, herbicides, and so on [1-5]. These compounds are typically produced by the selective catalytic hydrogenation of nitroarenes or nitroaromatics (Ar-NO$_2$) in the presence of hydrogen gas (H$_2$) by using catalysts such as metal, metal oxide, sulfide, and functional carbon material [3-5]. This reaction is normally operated under medium-to-high temperature and pressure [4, 5]. However, the safety issues associated with handling during plant scale production, flammable hydrogen gas, and high reaction temperature remain major concerns [2, 5, 6]. Furthermore, the development of high efficiency and selectivity for hydrogenation of Ar-NO$_2$ is one of the most important goals of the chemical industries [6]. For example, the selective hydrogenation of 3-nitrostyrene (3-NS) to 3-vinylaniline which is challenging because its two reducible functional groups can be hydrogenated. This reaction mechanism was proposed by Haber et al [4].

A photocatalytic system is an encouraging approach for green and organic synthesis which has recently attracted increasing attention due to its high safety, the broad range of its utilization, and clean process [1, 2, 5, 6]. Among various photocatalysts, titanium dioxide (TiO$_2$) has widely used owing to its high chemical stability, inexpensive, non-toxicity, and easily separated from the reaction mixture [1, 6-9]. The photocatalytic hydrogenation of Ar-NO$_2$ is generally carried out in organic solvents, which is regarded as a hole scavenger and hydrogen source. Alcohol is one of the most common solvents for this reaction because it is readily available and inexpensive [1, 2, 5-7, 10]. Upon light irradiation, electrons (e$^-$) are induced in the conduction band (CB) and holes (h$^+$) simultaneously generated in the valence band (VB), causing oxidation of alcohol to carbonyl compounds and reduction of Ar-NO$_2$ to

Ar-NH$_2$, respectively [1, 2, 5, 11, 12]. In addition, the presence of oxygen gas (O$_2$) must be avoided in the photocatalytic reduction because O$_2$ can compete with the reduction of substance [7, 13].

The photocatalytic performance of this reaction depends on both the catalysts and the reaction conditions [9, 14-16]. To improve the photocatalytic performance of TiO$_2$ for the selective hydrogenation of Ar-NO$_2$, the most popular method was the incorporating onto TiO$_2$ surface of either noble metal, such as Platinum (Pt), Silver (Ag), Gold (Au), and Palladium (Pd), or base metal such as Nickle (Ni) and Copper (Cu) nanoparticles [8, 15-19]. In the several reports, Pt/TiO$_2$ catalysts contribute to improving the activity and selectivity and activity by e$^-$ trapping with consequent enhancement of the charge separation to preventing the fast recombination of e$^-$ and h$^+$ pairs. Also, Pt-based TiO$_2$ catalyst is known to be effective for Ar-NO$_2$ hydrogenation to Ar-NH$_2$ because Pt selective to hydrogenate the N=O bond [15, 16, 18-24]. Besides, Pt metal has received attention due to its excellent reactivity and selectivity, low cost, high stability, and easy to access [20-22].

Several reports were extensively studied the photocatalytic hydrogenation of Ar-NO$_2$ in alcohol using nanoparticle catalysts. However, a deeper understanding of the influences for the photocatalytic hydrogenation of Ar-NO$_2$ is necessary to enhance the activity and selectivity of photocatalytic reactions upon the abbreviated duration of light irradiation [7]. The mechanism and reaction pathways of the selective photocatalytic hydrogenation of Ar-NO$_2$ over P25-TiO$_2$ in alcoholic solvents was not deeply studied. Moreover, the influence of the various conditions on the photocatalytic performance of the selective photocatalytic hydrogenation has been published only a few studies.

In this study, the mechanism and the reaction pathways of the selective photocatalytic hydrogenation of Ar-NO$_2$ over P25-TiO$_2$ in alcoholic solvents under UV light at room temperature and an inert atmosphere was investigated. Also, the factors, including the type of substrates, the amount of substrate and catalyst, type of alcoholic solvents, and the deposition of Pt on TiO$_2$ that affect the photocatalytic performance of the selective photocatalytic hydrogenation of Ar-NO$_2$ were examined.

1.2 Objectives

1. To study the mechanism and photocatalytic performance of the selective photocatalytic hydrogenation of different Ar-NO$_2$ to Ar-NH$_2$ in various alcoholic solvents, including ethanol, 2-propanol, and butanol under UV light irradiation using P25-TiO$_2$.

2. To investigate the effect of the deposition of Pt on P25-TiO$_2$ support on the photocatalytic activity.

1.3 Research scopes

1.3.1 Investigation of the mechanism and photocatalytic activity of the selective photocatalytic hydrogenation of Ar-NO$_2$ in alcohol solvent using P25-TiO$_2$ under UV light at room temperature and atmospheric pressure for 4 h.

1. To study the effect of type of Ar-NO$_2$ (Nitrobenzene and 3-Nitrostyrene) on the photocatalytic hydrogenation performance.

2. To study the effect of concentration of Ar-NO$_2$ on the photocatalytic hydrogenation performance.

3. To study the effect of type of alcoholic solvents (ethanol, 2-propanol, butanol) on the photocatalytic hydrogenation performance.

4. To study the effect of the deposition of Pt on P25-TiO$_2$, as prepared by the conventional incipient wetness impregnation method, on the photocatalytic hydrogenation performance.

1.3.2 Characterization of the P25-TiO$_2$ and Pt/P25-TiO$_2$ catalysts.

1. X-ray diffractometry (XRD)

2. Nitrogen physisorption

3. Inductively coupled plasma-atomic emission spectroscopy (ICP-AES)

4. Scanning electron microscope and Energy dispersive X-ray spectroscopy (SEM-EDX)

5. UV-visible diffuse reflectance spectroscopy (UV-Vis)

6. X-ray photoelectron spectroscopy (XPS)

7. Photoluminescence spectroscopy (PL)

CHAPTER 2
THEORY AND LITERATURE REVIEW

2.1 Titanium dioxide

Photocatalysts are photosensitive semiconductor materials such as titanium dioxide (TiO_2), zinc oxide (ZnO), cerium dioxide (CeO_2), cadmium sulfide (CdS), zinc sulfide (ZnS), etc. These may be used as a pure metal oxide or doped oxides. TiO_2, also known as titanium (IV)oxide or titania, is one of the most investigated semiconductors since the discovery of its water splitting property and photocatalytic decomposition in the 1970s [12, 25]. Owing to the abundance, chemical stability, inexpensive, and non-toxicity for human and environmental, TiO_2 has widely used for applications in catalysis, cosmetics, pigments and paints, dye-sensitized solar cells (DSSCs), antibacterial agents, environmental purification, self-cleaning and self-sterilizing solid surfaces, and so on [25, 26]. For these technologies, it is typically necessary to use powerful ultraviolet (UV) light or solar light sources [26]. The properties of TiO_2 are shown in Table 1.

Table 1 The chemical and physical properties of titanium dioxide (TiO_2) [27].

Properties	TiO_2
Molecular weight	79.866 g/mol
Melting point	1844 °C
Boiling point	2973 °C
Refractive index	Anatase
	Rutile
	Brookite
Appearance	White solid
Solubility	Insoluble in water
Odor	Odorless

TiO_2 is regarded as semiconductors, in which electrons (e^-) and holes (h^+) simultaneously photogenerated in the conduction band (CB) and valence band (VB),

respectively, play important roles in electroconductivity as well as chemical reactivities on the surface. One of the main points in the semiconductor photocatalyst TiO_2 is band gap energy between CB and VB and potential energy levels of CB and VB which photogenerated electrons and holes can quench quickly due to the charge recombination [12]. Some researchers have studied to reduce the recombination of electron-hole pairs to enhance the photocatalytic activity of TiO_2.

There are three main types of TiO_2 crystalline phases containing rutile, anatase, and brookite, as seen in Figure 1 and Table 2. The particles size, in which the most stable phase, of rutile, anatase, and brookite is above 35 nm, below 11 nm, in the range 11 - 35 nm, respectively. Brookite phase has an orthorhombic structure which is rare and difficult to prepare while both anatase and rutile phases have a tetragonal structure. For crystal structures, rutile has three main crystal faces: (110), (100), and (001) and anatase has three main index faces: (101), (100), and (001) which (101) and (001) are common for natural crystals [12, 26]. Both rutile and anatase TiO_2 in the form of powders can transform into other phases at temperatures above 600 ºC [26, 28]. Each phase has different activities for photocatalytic reactions. However, rutile and anatase have been mainly used as photocatalysts in practical work. Anatase and rutile phases reveal definite band gap energy at around 3.2 eV and 3.0 eV, respectively. The band gap of anatase is slightly larger than that of rutile since the CB level of anatase is located at 0.2 eV more negative than that of rutile as shown in Figure 2.
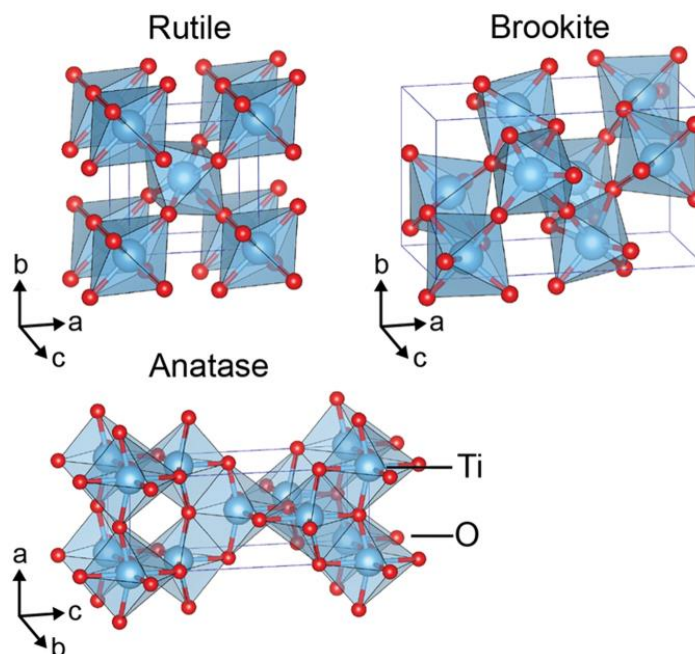
Figure 1 Crystal structures of TiO$_2$ [7].

Table 2 The properties of different TiO$_2$ polymorphs [27].

Phase	Crystal system	Density (g/cm^3)	band-gap (eV)	Refractive index
Rutile	Tetragonal	4.13–4.26	3.0	2.72
Brookite	Orthorhombic	3.99–4.11	3.11	2.63
Anatase	Tetragonal	3.79–3.84	3.19	2.52
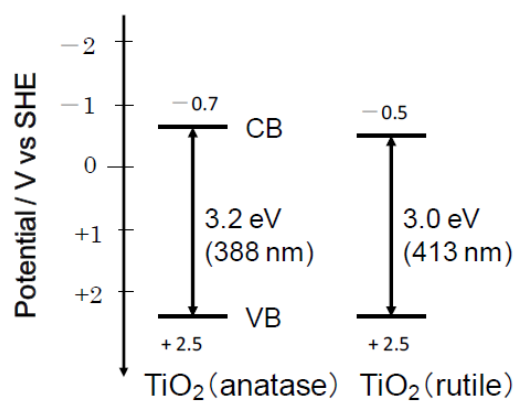
Figure 2 Band gaps and band edge positions of TiO$_2$ photocatalysts [11].

Degussa P25 (Aeroxide TiO_2) is a commercial TiO_2 photocatalyst that is composed of anatase and rutile crystallites in ratio 3:1. The average particle sizes of P25-TiO_2 is 25nm, P25-TiO_2 induce the high photocatalytic activity more than pure phase due to interface anatase and rutile. Also, the mixed-phase P25 is used widely because of its relatively high levels of activity in many photocatalytic applications [8, 28]. The microstructure of P25-TiO_2 was shown in Table 3.

Table 3 The microstructure and properties of commercial P25-TiO_2 [2, 29].

Parameter (test method)	Commercial P25-TiO_2
Anatase component (%)	83
Rutile component (%)	17
Anatase crystallite size (nm)	20.8
Rutile crystallite size (nm)	30.5
BET surface area ($m^2 g^{-1}$)	51.46
Total pore volume ($cm^3 g^{-1}$)	0.17

2.2 Fundamentals of catalytic hydrogenation of nitroaromatics

Aniline and functionalized aniline is produced by the hydrogenation of nitroaromatics. This product is an important intermediate for the production of various chemicals, such as polymers, pigments, pharmaceutical, and herbicide. More than a decade ago, the reaction network for the hydrogenation of nitrobenzene and substituted nitrobenzene was proposed by Haber et al [5, 30], as shown in Figure 3-4. This mechanistic scheme is an excellent basis to describe how the catalytic hydrogenation proceeds. Two different reaction pathways to aniline are recommended, in which nitrosobenzene, phenylhydroxylamine, azobenzene, azoxybenzene, and hydrazobenzene are intermediates. Generally, the nitroso intermediate presents in trace concentration and hydroxylamine concentration varies considerably depending on such factors as substrate structure, reaction temperature, hydrogen pressure, solvents, catalysts, and pH value. The reaction profile indicates fast hydrogenation of the nitro

group to nitroso intermediate, which is absorbed very strongly on the catalyst surface and hydrogenated to hydroxylamine fast, and the hydrogenation of hydroxylamine to aniline is the rate determining step. Another pathway, condensation to azo and azoxy products do not usually occur, through the intermolecular dehydration between nitrosobenzene and hydroxylamine [5]. In the case of 3-nitrostyrene hydrogenation, the reaction pathways are consistent with the nitrobenzene hydrogenation. Besides, 3-ethylnitrobenzene (3-ENB) and 3-ethylaniline (3-EA) were generated as byproducts. This because the vinyl group (C=C) of 3-NS was reduced to produce 3-ENB. Then, the further hydrogenation of 3-VA and 3-ENB can occur and promptly convert to 3-EA [4].
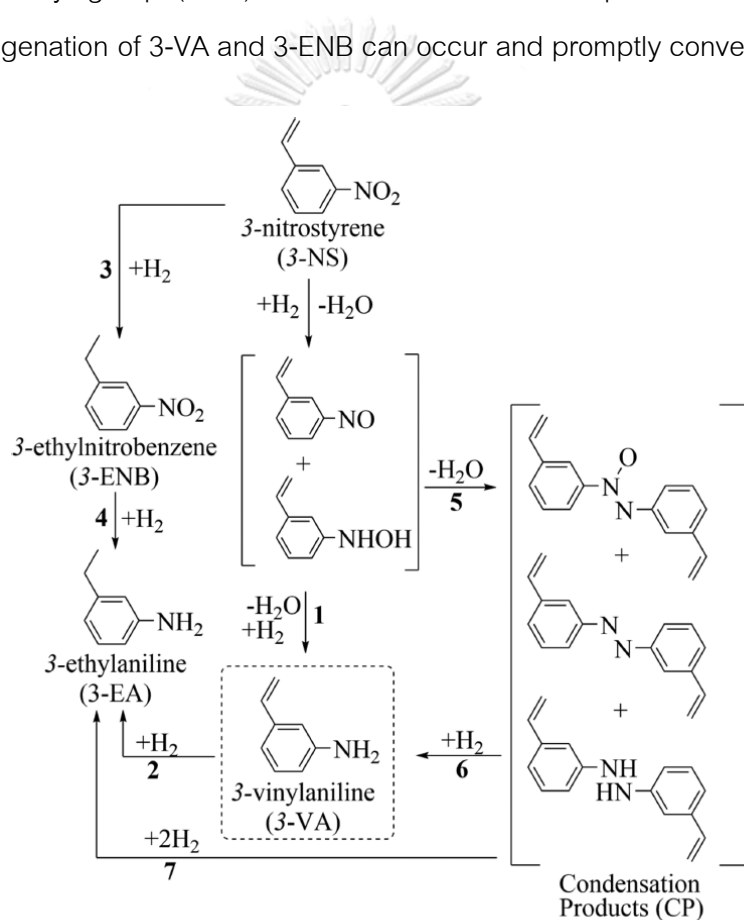
Figure 3 Mechanism reaction route for the hydrogenation of 3-nitrostyrene proposed by Haber [4].
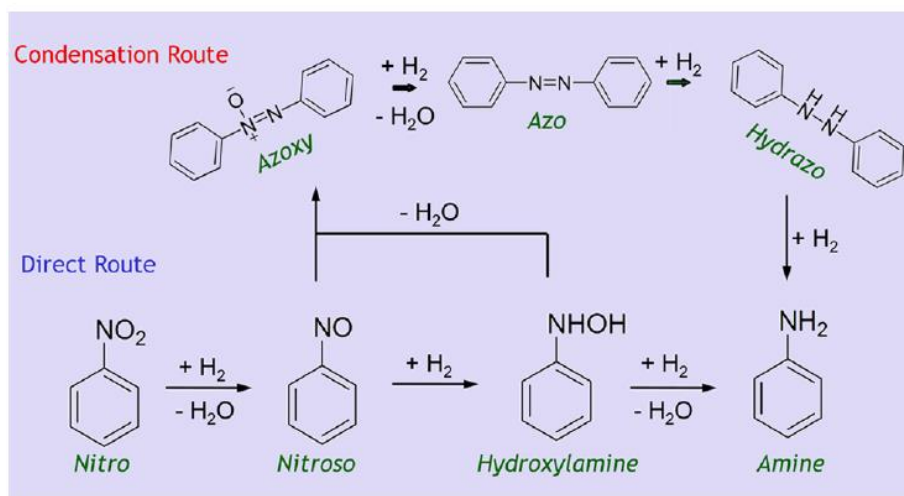
Figure 4 Mechanism reaction route for the hydrogenation of nitrobenzene proposed by Haber [30].

AR-NO$_2$ hydrogenation reactions generally require three components, including the substrate, the hydrogen source, and a catalyst. These hydrogenation reactions will not occur between hydrogen and organic compound below 480°C without metal catalysts. Moreover, these reactions also not occur when a semiconductor without metal doping used as a catalyst [3, 4, 31, 32]. Thus, the metal catalysts are required in the reaction to promote activity and chemoselective products. Catalytic hydrogenation reactions are affected by many factors, which include the presence of catalytic activators or poisons, temperature, pressure, solvent agitation and other conditions specific to the process [33]. The liquid phase hydrogenation of Ar-NO$_2$ with high temperature and hydrogen pressure conditions was studied by several researchers.

Berguerand, C. et al. [4] studied hydrogenation of 3-nitrostyrene to 3-vinylaniline over platinum nanoparticles supported on several metal oxides. The liquid phase hydrogenation reactions were carried out in a reactor equipped with a pressure-controlled H$_2$ supply system containing ethanol as a medium solvent under H$_2$ atmosphere at 10 bar and T = 348 K. The results showed that both nitro group (N=O) and vinyl group (C=C) can be reduced. The observed difference in the reaction pathways of 3-NS hydrogenation over Pt nanoparticles can be attributed to the support

used and a difference in modes of 3-NS adsorption on Pt active sites. It was observed that TiO_2, Fe_2O_3, and ZnO exhibited a higher selectivity toward 3-VA, while Al_2O_3 and carbon material gave 3-EA as the only product.

Pt metal based TiO_2 catalyst was popular in 3-NS hydrogenation to 3-VA because Pt selective to hydrogenate the N=O bond. According to Yoshida, H. et al [18], supported Pt catalysts were prepared using different crystallite size TiO_2 supports and their catalytic activity was tested for the liquid phase hydrogenation of 3-NS and NB. This reaction was operated at 323K and H_2 pressure at 40 bars. With Pt on smaller TiO_2 crystallites, the selectivity of 3-VA was improved in the hydrogenation of 3-NS, promoting its regioselective hydrogenation. These because nanocrystal TiO_2 support led to low coordinated and/or electron-rich Pt site, which was more active for the hydrogenation of the nitro group than the vinyl group.

2.3 Photocatalytic hydrogenation of nitroaromatics

Photocatalyst semiconductor is a critical substance for photocatalytic reaction owing to it can be chemically stimulated by light irradiation. The field of heterogeneous photocatalysis is interesting as shown by the number of papers reporting and extensively studied due to the broad range of its utilization. Understanding of solid-state chemistry such as crystal structure, electronic conductivity, chemical bonds and structure and arrangements of atoms are important for the mechanisms in heterogeneous photocatalysis. Photocatalytic hydrogenation of ethene and ethyne firstly reported by Boonstra and Mutsaers in 1975s which some hydrogenated products have been detected upon the UV illumination (320 – 390 nm) of P25-TiO_2 in an atmosphere of ethene or ethyne [34]. Several organic nitroaromatics can be easily hydrogenated to provide corresponding amino compounds in the presence of sacrificial hole scavenger upon the UV irradiated TiO_2 photocatalyst as firstly reported by Mahdavi et al [20]. Since then, the photocatalytic hydrogenation of nitro compounds using some kinds of semiconductor photocatalysts was extensively studied.

The photocatalytic hydrogenation can be carried out in the presence of electron donors and in the absence of molecular oxygen (O_2). The intention of using the electron donors is to scavenge generated holes in the valence band, by which abbreviating the level of recombination between e^- and h^+ within the semiconductor photocatalysts. Therefore, choosing an appropriate electron donor as hole scavengers is important for the hydrogenation of organic substrates [12]. The photocatalyst is the key to produce hydrogen species from the hydrogen donors that is also called hole scavenger or an electron donor such as alcohols, ammonium formate, oxalic acid, and so on [1, 12].

The photonic activation of photocatalyst is important for photocatalytic reaction. The electronic band structure of the photocatalyst consists of the valence band (VB) and conduction band (CB). The valence band was the highest occupied band while the conduction band was the lowest occupied energy band [35]. In addition, the band gap energy defines the minimum photon energy absorbed by the semiconductor photocatalysts or difference in energy between valance band (VB) and conduction band (CB) which driving force for transfer electron or hole when TiO_2 activated by light [12, 36] The adequate energy, that must be supplied by the photon from the light source for the promotion of the electrons and occurrence of photocatalytic reactions, should be equal to, or greater, than the band gap energy of photocatalysts [12, 36, 37]. The irradiation of the surface of the TiO_2 produces the separation of two types of carriers that are an electron (e^-) and a hole (h^+). An electron from the valence band transfers to the conduction band, leaving an electron deficiency or hole in the valence band and then these electrons and holes can participate in redox reaction, in which the hole can oxidize an organic molecule adsorbed on the TiO_2 surface and the electron in the conduction band can reduce an organic molecule [36, 37]. A schematic of the photocatalytic mechanism where excitation of electrons on the catalyst form electrons and holes (charge carriers) as depicted in Figure 5. Moreover, the formation of hydrogen species and activation of the substance in other hydrogenation routes, and charge separation and combination are determining factors for the overall hydrogenation activity [5].
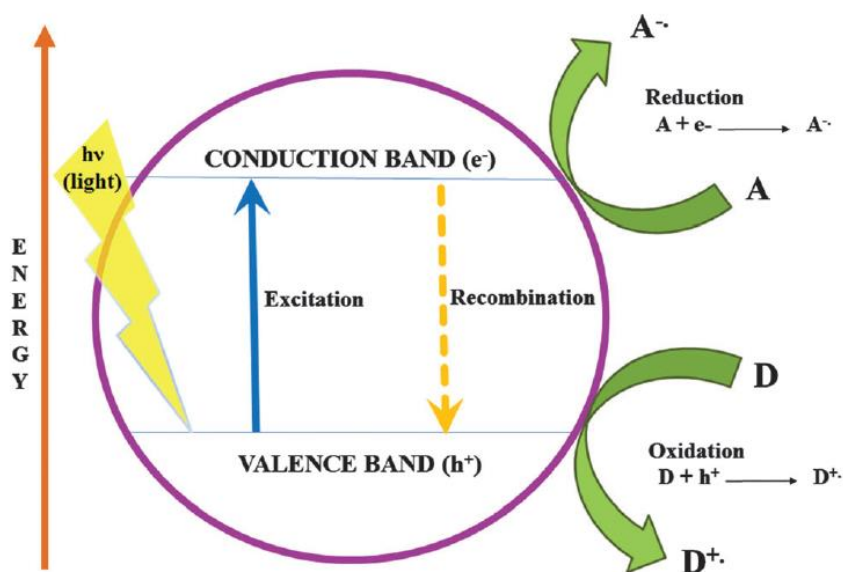
Figure 5 A schematic of the photocatalytic mechanism [36].

The photocatalytic reaction is an alternative process for nitroaromatics hydrogenation reaction because it is a safe and green process. The photocatalytic hydrogenation of nitroarenes by TiO_2 using alcohol as a hydrogen source under atmospheric pressure and room temperature can induce both oxidative and reductive products. The photooxidation of alcohols produces carbonyl compounds such as aldehydes and ketones, while the photoreduction of nitroarenes generates the corresponding functionalized aniline or amine compounds [1, 2, 7]. From reaction routes for the photocatalytic hydrogenation of $Ar-NO_2$ to $Ar-NH_2$ were presented in Figure 6. Additionally, the following sections describe five steps of the photocatalytic process as shown in Equation (1) to (5).

$$TiO_2 + h\nu \rightarrow h^+ + e^- \tag{1}$$

$$(CH_3)_2CHOH \xrightarrow{2h^+} (CH_3)_2CO + 2H^+ \tag{2}$$

$$Ar-NO_2 \xrightarrow{2e^-, 2H^+} Ar-NO + H_2O \tag{3}$$

$$Ar-NO \xrightarrow{e^-, H^+} [Ar-NOH^\bullet] \xrightarrow{e^-, H^+} Ar-NHOH \tag{4}$$

$$Ar-NHOH \xrightarrow{e^-, H^+} [Ar-NH^\bullet] + H_2O \xrightarrow{e^-, H^+} Ar-NH_2 \tag{5}$$
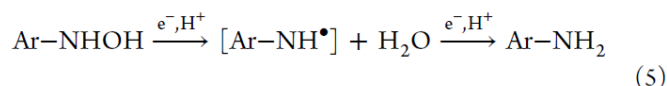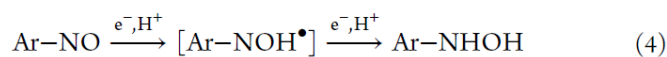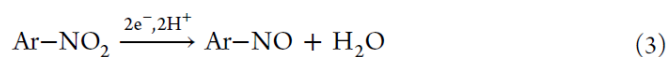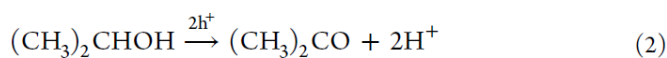
Figure 6 Reaction pathways for the photocatalytic hydrogenation of Ar-NO$_2$ in 2-Propanol using TiO$_2$ [2].

Step 1

The photo-excited charged carriers occurred when photon energy equal or higher band gap energy. The e$^-$ was excited and transferred from VB to CB, while h$^+$ was simultaneous generated in VB, as shown in Equation (1).

$$TiO_2 + h\nu \longrightarrow TiO_2 \ (e^- + h^+) \tag{1}$$

However, e$^-$ and h$^+$ could recombine in bulk or surface of catalyst because the excited e$^-$ was easily transferred back to VB (Ground state). This phenomenon led to energy release [35].

Step 2

For this process, alcohol served as hole scavenger in the photocatalytic oxidation. Upon irradiation, alcohol was oxidized by h$^+$ to produce carbonyl compound and release proton or hydrogen species (H$^+$), as shown in Equation (2).

$$(CH_3)_2CHOH \longrightarrow (CH_3)_2CO + 2H^+ \tag{2}$$
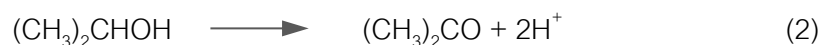
Step 3-5

Steps 3 to 5 were the photocatalytic reduction of Ar-NO$_2$ on the surface of TiO$_2$. Ar-NO$_2$ was reduced by e$^-$ and H$^+$ to Ar-NO, Ar-NHOH, and Ar-NO$_2$, respectively.

The overall step of photocatalytic hydrogenation reaction is concluded as shown in Equations (3) to (5) in Figure 6.

$$\text{Ar-NO}_2 + 3(\text{CH}_3)_2\text{CHOH} \longrightarrow \text{Ar-NH}_2 + 3(\text{CH}_3)_2\text{CO} + 2\text{H}_2\text{O}$$

The photocatalytic hydrogenation of Ar-NO$_2$ in several solvents such as alcohols using TiO$_2$ catalysts was reported by several authors.

Imamura, K. et al. [13] examined the photocatalytic reduction of *m*-nitrobenzenesulfonic acid (*m*-NBS) in aqueous suspensions of TiO$_2$ in the presence of formic acid (FA) utilization as hole scavengers under deaerated conditions. It was found that *m*-NBS was almost quantitatively reduced to *m*-aminobenzenesulfonic acid (*m*-ABS) as the final product. The *m*-NBS was continuously consumed whereas *m*-nitrosobenzenesulfonic acid (*m*-NSBS) and *m*-hydroxylaminesulfonic acid (*m*-PHAS) were formed as intermediate along with the irradiation time. After photoirradiation, *m*-ABS was obtained almost quantitatively, indicating that no side reaction of *m*-NBS and intermediates occurred in this system. Moreover, CO$_2$ was generated as the oxidized product by photooxidation of formic acid, which CO$_2$ could be liberated in the gas phase because of the acidic condition of this reaction system. In addition, photocatalytic reduction of *m*-NBS to *m*-ABS using TiO$_2$ samples with various specific surface areas was examined to determine the effect of *m*-NBS adsorption on the TiO$_2$ surface on the yield of *m*-ABS. The result showed that a large surface area of TiO$_2$ causing a large amount of adsorption of *m*-NBS is an important factor for high yield of *m*-ABS in photocatalytic reduction of *m*-NBS.

Moreover, another research by Imamura was reported. Imamura, K. et al. [1] studied the photocatalytic reduction of nitrobenzene and nitrobenzene with other reducible groups such as chloro, vinyl, and bromo in 2-propanol suspensions of TiO$_2$ under air and deaerated conditions. From the results in the absence of O$_2$, nitrobenzene was consumed, while aniline and acetone were produced as the photoreduction product of nitrobenzene and the photooxidation product of 2-propanol, respectively. Also, the color of TiO$_2$ became blue, indicating that a part of Ti^{4+} in TiO$_2$ was reduced to Ti^{3+}. Furthermore, only the nitro group of these compounds was selectively reduced even in the presence of chloro, vinyl, and bromo groups without reductive dehalogenation, resulting in the production of corresponding amino compounds with

high yields. For the photocatalytic reaction under air, aniline was formed slightly less than while acetone was formed much more than the results under deaerated conditions, indicating that holes oxidized 2-propanol to acetone and electrons were trapped by O_2, and oxidized 2-propanol, not aniline. However, the photocatalytic reduction system has been generally operated under vacuum or inert gases such as nitrogen and argon because oxygen behaves as a strong acceptor of photogenerated electrons and reduces the efficiency of photocatalytic reduction in the target substrate.

Shiraishi, Y. et al [2] reported the highly efficient and selective hydrogenation of nitroaromatics on photoactivated rutile titanium dioxide. This reaction is carried out in isopropanol, serves as a hole scavenger, containing nitroaromatics at room temperature and inert gas (N_2) atmosphere. TiO_2 was activated by irradiation of UV light ($\lambda > 300$ nm) and then photoexcited TiO_2 induce electron (e^-) and positive hole (h^+) pairs in the conduction band and the valence band. Ti^{3+} atoms which located at the surface vacancies are the active sites for nitro compounds hydrogenation on rutile TiO_2, as shown in Figure 7. The Ti^{3+} atoms on TiO_2 surface work as the adsorption site for nitroaromatics via electron donation and as the trapping site for a photoinduced electron. These effects promote fast and selective nitro-to-amine hydrogenation of the adsorbed nitroaromatics by the surface-trapped electrons. The photocatalytic hydrogenation of rutile TiO_2 system enables significantly high selectivity of aniline and functionalized aniline and can be carried out with a non-noble metal catalyst at room temperature and atmospheric pressure.
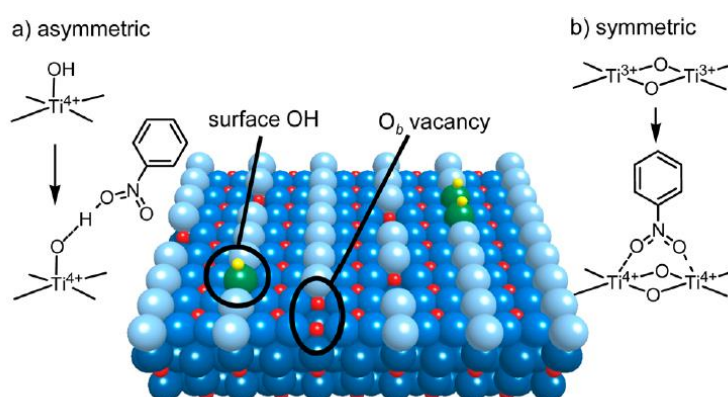
Figure 7 Surface structure of rutile TiO_2 and adsorption modes of nitrobenzene

Hakki, A. et al. [7] studied the photocatalytic conversion of various nitroaromatic compounds with alcohols containing different types of TiO_2. Upon illumination of a solution of nitroaromatics and ethanol solvent in the presence of the bare TiO_2 photocatalyst, different products were obtained. Before illumination, the reactor was placed in a sonicator and then purged with argon gas (Ar) until no oxygen since O_2 competes to trap electrons with the nitroaromatic compounds. A simultaneous reduction of the nitro compounds is induced by photogenerated electrons and oxidation of the alcohol is produced by the formed holes in all cases. A primary amino compound, namely primary amine, such as aniline was products of the reduction of nitroaromatics. Also, imine which is generated by condensation of amino compounds and produced carbonyl compounds is other products. Base on the results over different types of TiO_2, rutile TiO_2 enhanced highly selectivity primary amino compounds while anatase TiO_2 provided a mixture of imines and amino compounds. It concluded that the surface properties of the photocatalysts play a significant role in the reaction pathway and thus affected in the selectivity of the products.

Kaur, J. et al. [8] investigated the photocatalytic activity of the selective reduction of *m*-dinitrobenzene in isopropanol using the several metals (Au, Ag, Pt, and Pd) loaded P25-TiO_2 catalysts under UV light irradiation. For Pt loaded-TiO_2 catalyst, Pt loading led to lower PL intensity and higher band gap energy as compared to bare P25-TiO_2 catalyst. Upon irradiation, the metal-deposited P25-TiO_2 catalysts produced *m*-nitroaniline as a major product after 4 h of UV light irradiation. Meanwhile, the bare P25-TiO_2 catalyst selectively produced 100% *m*-phenylenediamine. Furthermore, the plasmonic interaction of Pt having characteristics absorption bands in the UV light region could impart crucial effects on the charge transfer for enhancement activity of the catalyst.

Nakai, Y. et al. [38] synthesized the imines from the photocatalytic reaction of several benzylic alcohols with nitrobenzene using the CdS-sensitized TiO_2 (CdS-TiO_2) photocatalyst under visible-light irradiation at room temperature. Also, the solvent effects on the production of imines were examined. The solvents were classified into three

categories, including protic polar solvents (ethanol and water), aprotic polar solvent (acetonitrile) and non-polar aprotic solvents (toluene, cyclohexane, and n-hexane). The results showed that the imines were formed in several solvents except for water. The yields of imines formation were significantly influenced by the solvents as followed: ethanol < acetonitrile < cyclohexane. This indicated that the condensation reactions between benzaldehyde and aniline effectively take place in the non-polar solvents. Therefore, the photocatalytic activity of the synthesis of imines depended on the electric nature of the benzylic alcohols. This photocatalytic system consists of four steps as shown in Figure 8.
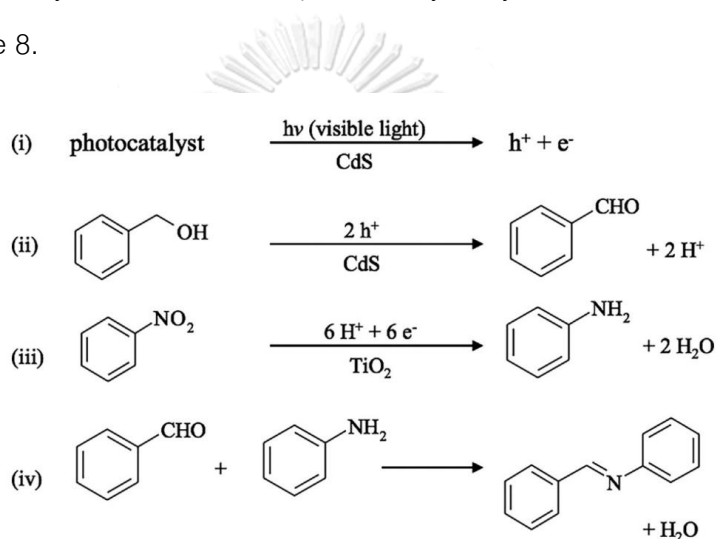
Figure 8 Synthesis of imine from benzyl alcohol and nitrobenzene on the CdS-TiO$_2$ photocatalyst under visible-light irradiation.

Flores, S. O. Et al [11] studied the photocatalytic reduction of nitrobenzene to aniline in a large excess of ethanol as a sacrificial electron donor using TiO$_2$ catalyst under UV light irradiation for 4 h in order to identify the reaction pathway and formed by-products. Upon irradiation, aniline and acetaldehyde were produced as the main products. However, by-products were also formed such as imines and quinolines. Imines were produced by the condensation of aniline and acetaldehyde. Also, indoles and quinolines can be produced as by-products, probably due to the reaction between strongly adsorbed aniline and the subsequent reactive intermediates of ethanol photo-oxidation catalyzed by TiO$_2$.

Furthermore, the photocatalytic process for the H_2 gas production in alcohol solvents using TiO_2 catalysts was also reported by several authors.

Chiarello, G. L. et al [21] studied the photocatalytic production of hydrogen by methanol steam reforming over a series of pristine or noble metal (Ag, Au, Au–Ag alloy and Pt) – modified TiO_2 photocatalysts, which synthesized by the deposition of metal nanoparticles on TiO_2. The fed gas mixture was methanol and water vapors. Hydrogen gas evolved at a constant rate, which significantly increased upon noble metal addition. Pt confirmed to be the most effective co-catalyst also for this gas phase reaction.

จุฬาลงกรณ์มหาวิทยาลัย
CHULALONGKORN UNIVERSITY

CHAPTER 3
EXPERIMENTAL

This chapter describes the details of materials and chemicals, preparation and characterization of catalyst, and photocatalytic reaction test.

3.1 Materials and chemicals

Table 4 Lists of chemicals for this photocatalytic hydrogenation reaction

Chemicals	Formula	Suppliers
Titanium dioxide (P25 grade)	TiO_2	Degussa
Nitrobenzene	$C_6H_5NO_2$	Sigma-Aldrich
3-Nitrostyrene	$C_8H_7NO_2$	Sigma-Aldrich
Aniline	$C_6H_5NH_2$	Sigma-Aldrich
3-Vinylaniline	$C_8H_7NH_2$	Sigma-Aldrich
Ethanol	C_2H_5OH	Merck
2-propanol	$(CH_3)_2CHOH$	Fisher Chemical
Butanol	$C_4H_{10}O$	Fisher Chemical
Acetaldehyde	C_2H_4O	Sigma-Aldrich
Acetone	$(CH_3)_2CO$	Merck
Butanone	C_4H_8O	Sigma-Aldrich

3.2 Preparation of Pt/P25 catalyst

Degussa P25-TiO_2 was used as the catalyst support. Pt/P25 catalyst was prepared by the conventional incipient wetness impregnation method, as shown in Figure 9. P25-TiO_2 powder was impregnated with an aqueous solution of platinum precursor. This Pt precursor solution was gradually dropped onto the P25-TiO_2 support to get 0.6 %wt. Pt/P25, as the desired Pt content. The obtained samples were dried in an oven at 110 °C overnight and then calcined in a muffle furnace at 400 °C under an air flow with a heating rate 10°C/min for 2 h.
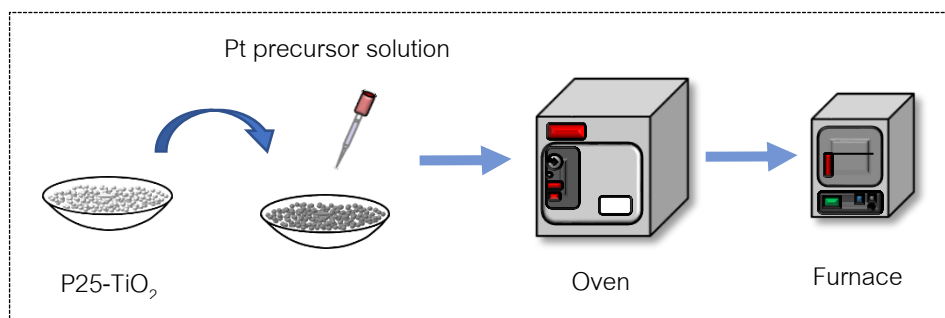
Figure 9 Scheme of preparation Pt deposited TiO_2 catalyst by the incipient wetness impregnation method.

3.3 Photocatalytic reaction tests

The typical photocatalytic hydrogenation reaction was carried out in a cylindrical quartz reactor with a total volume of 400 cm^3. 0.2 g of TiO_2 photocatalyst was taken into a stirred slurry reactor. Next, nitroaromatic was dissolved in 40 cm^3 of alcohol solvent and subsequently added to above quartz reactor. This quartz reactor was sealed with a septum cap, sonicated for 5 min to disperse catalyst well and then purged with N_2 for 5 min. The reaction was started by turning on the UV light, which was photo-irradiated from the outside, using UV-light bulbs (Philips Germicidal Ozone UV Quartz Glass UVC Bulb; 16 Watts; 6 bulbs) with magnetic stirring at atmospheric pressure and room temperature. Schematic diagram of photocatalytic hydrogenation reaction was presented in Figure 10. During the reaction, the resulting mixture was collected every 30 minutes of the irradiation time for 4 h and was separated from the irradiated mixture by filtration via a 0.2 μm filter. The liquid sample was analyzed by gas chromatography (GC) equipped with FID and TCD detector. The reactant and product concentrations were calibrated with authentic samples. The properties and conditions for GC operation were summarized in Table 5. In addition, the effect of several conditions, including reactants, the concentration of reactant, alcoholic solvents, and the deposition of Pt on TiO_2 on photocatalytic activity were tested in a similar way to the above-mentioned experiment.

Table 5 Conditions of Gas-Chromatography

Gas chromatography	Shimadzu GC-2014	Shimadzu GC-2014	Shimadzu GC-8A
Detector	FID	FID	TCD
Packed column	Rtx®5	DB1-Wax	Molecular sieve 5A
Carrier gas	He (99.99 vol. %)	He (99.99 vol. %)	Argon
Make-up gas	Air (99.9 vol. %)	Air (99.9 vol. %)	-
Column temperature	140°C	45°C	70°C
Injector temperature	270°C	230°C	100°C
Detector temperature	310°C	250°C	100°C
Time analysis	20 min	6 min	5 min
Analyzed product	Ar-NO$_2$, Ar-NH$_2$ Alcohol	Alcohol, Carbonyl compound	H$_2$
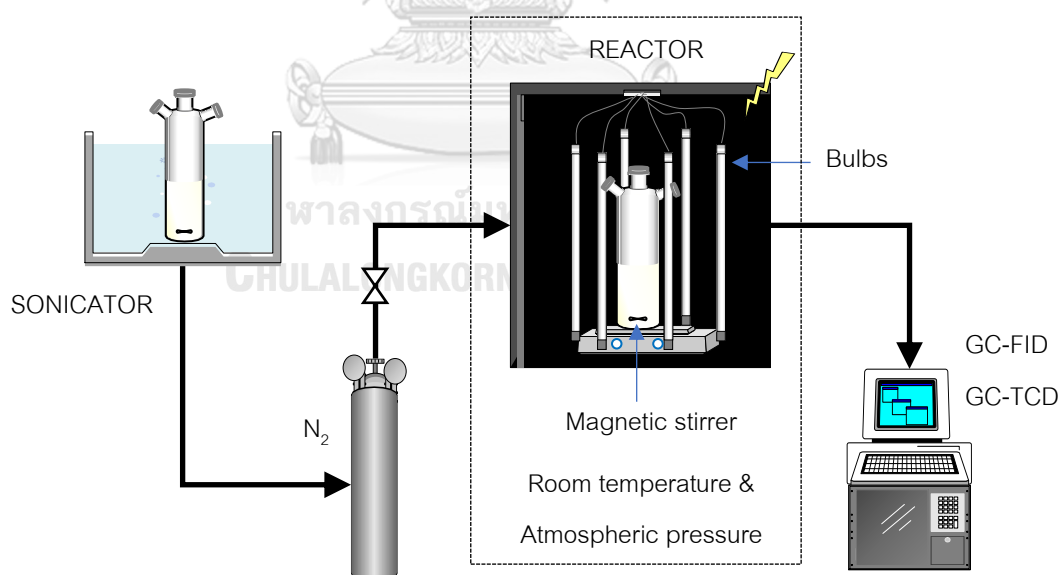
Figure 10 Schematic diagram of photocatalytic hydrogenation reaction.

3.4 Catalyst characterization

3.4.1 X-ray diffractometry (XRD)

The X-ray diffraction (XRD) pattern was presented using a SIEMENS D5000 X-ray diffractometer with Cu K$_\alpha$ irradiation and a Ni filter in the range between 20° to 80°. Also, the scan speed was 0.5 sec/step and a slit width was 0.6 mm. The crystallite size of the catalyst was calculated by the Debye-Scherrer equation.

3.4.2 Nitrogen physisorption

The specific surface area of catalysts was measured in a Micromeritics ASAP 2020 instrument. The mixture of nitrogen gas and helium gas (30%:70%) was used as a carrier gas in this technique. Also, liquid nitrogen was used in the catalyst adsorption process. After analysis, the amounts of nitrogen adsorption and desorption were determined to calculate BET specific surface area by the single-point method.

3.4.3 Inductively coupled plasma-atomic emission spectroscopy (ICP-AES)

Inductively coupled plasma-atomic emission spectroscopy (ICP-AES) was performed by using a 2100 DV spectrometer to measure the amount of deposited Pt on the TiO$_2$ surface. For sampling preparation, the modified-TiO$_2$ powder was digested in a solution of sulfuric acid (97%, H$_2$SO$_4$) and DI water.

3.4.4 Scanning electron microscope and Energy dispersive X-ray spectroscopy (SEM-EDX)

SEM-EDX was used to investigate the morphology and the elements on the surface of the catalysts by using JEOL model JSM-5800LV. The powder sample must be dried in an oven at 110 °C overnight before SEM-EDX analysis.

3.4.5 UV-visible spectroscopy (UV-Vis)

The UV-visible spectroscopy was used to determine the light absorption spectra of TiO$_2$ catalyst, covering the wavelength range of 200-800 nm. This technique was

operated in the Perkin Elmer Lambda 650 UV-Vis spectrophotometer. In addition, the UV-vis spectrum was also used to calculate the band gap energy of TiO_2 photocatalyst.

3.4.6 X-ray photoelectron spectroscopy (XPS)

XPS analysis, as performed by using the KRATOS AMICUS X-ray photoelectron spectroscopy, used to investigate the surface composition and chemical states of elements and the binding energy of catalysts. This technique was operated with an Mg Kα X-ray as a primary excitation and KRATOS VISION II software. For TiO_2 catalyst, the binding energy of Ti 2p, O 1s were presented. Moreover, the powder sample must be dried at 110 °C overnight before analysis.

3.4.7 Photoluminescence spectroscopy (PL)

Photoluminescence spectroscopy was used to investigate the charge separation of photogenerated electron and hole and charge-carrier lifetimes of catalyst, as performed by Horiba 4P-Fluoromax spectrofluorometer. For this technique, a Xenon lamp was used as the excitation source with an excitation wavelength of 325 nm at room temperature.

CHAPTER 4
RESULTS AND DISCUSSION

In this chapter, the physiochemical properties and photocatalytic performance over P25-TiO$_2$ and Pt/P25 are discussed. The results and discussion are classified into two parts. Firstly, the deposition of Pt nanoparticles onto P25-TiO$_2$ support are studied. The characterization techniques for the Pt/P25-TiO$_2$ including XRD, ICP, BET surface area, UV-Vis, XPS, photoluminescence spectroscopy, and SEM-EDX are described. Secondly, the photocatalytic performance of catalysts for the selective photocatalytic hydrogenation of nitroaromatics in alcoholic solvents is reported. Also, the effect of several conditions, including reactants (nitrobenzene and 3-nitrostyrene), the concentration of reactant, alcoholic solvents (ethanol, 2-propanol, and butanol), and the deposition of Pt onto P25-TiO$_2$ on photocatalytic activity are presented.

4.1 The characterization of P25-TiO$_2$ and Pt/P25 catalysts

The X-ray diffraction technique was used to analyze the crystalline size, structure, and phase composition of TiO$_2$ catalysts. The XRD patterns of pure P25-TiO$_2$ and prepared Pt/P25 catalysts were shown in Figure 11. P25-TiO$_2$ catalyst consists of two mixture phases, containing the anatase and rutile phases. XRD pattern of P25 catalyst presented the characteristic main peaks for the anatase (101) phase at $2\theta = 25.3°$ and rutile (110) phase at $2\theta = 27.4°$. Moreover, the XRD peaks at 2θ equal to 25.3º, 37.8, 48.1º, 54.0º, 55.0º, 68.9º, 70.2º, and 75.3º were assigned to anatase phase. Meanwhile, the XRD peaks at 27.4º, 36.1º, 41.2º, 56.5º, and 62.7º were assigned to rutile phase [24, 31, 39, 40]. Pt/P25 catalyst exhibited the same characteristic peaks of the anatase and rutile phase as pure P25-TiO$_2$, indicating that the catalyst maintained the crystallite structure after deposition of Pt. The XRD peaks corresponding to Pt crystallites in Pt/P25 catalyst were not observable which resulted from the low amount of Pt loading and/or high dispersion of Pt on the surface of TiO$_2$ supports.

The phase composition and average crystallite sizes of TiO$_2$ were calculated from the XRD results, as summarized in Table 6. For the phase composition, the amount

of anatase and rutile phases was calculated from the areas of a major phase of the anatase (2θ = 25.3°) and rutile (2θ = 27.4°). Pt/P25 catalyst consisted of anatase phase ≈ 82% and rutile phase ≈ 18% contents which were approximate to that found for the pure P25-TiO$_2$ support.

The average crystallite sizes of all catalysts, which were estimated from the anatase peak (101) and rutile peak (110) according to methods of the Debye–Scherrer equation, were almost the same at around 24 nm. Accordingly, it can be concluded that the deposition of Pt onto P25-TiO$_2$ support did not affect the crystalline structure, crystallite size, and phase composition of TiO$_2$ support.
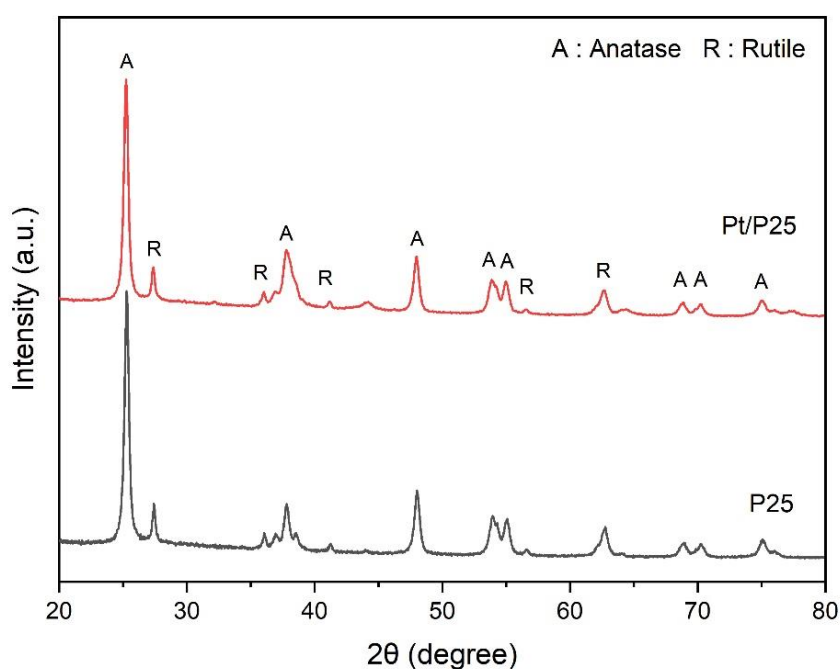

Figure 11 XRD pattern of pure P25-TiO$_2$ and prepared Pt/P25

Table 6 Crystallite sizes and phase composition of P25-TiO$_2$ and Pt/P25.

Catalysts	Crystalline size (nm)	Phase composition (%)	
		Anatase phase	Rutile phase
P25	24.2	82	18
Pt/P25	24.6	81	19

The Pt loading content of prepared Pt/TiO$_2$ catalysts was measured by using Inductively coupled plasma atomic emission spectroscopy (ICP-AES), as shown in Table 7. The results indicated that the Pt loading content was slightly less than expected value due to errors from the preparation of modified TiO$_2$ and the sample preparation for ICP analysis. However, it can be confirmed the loading of the catalysts amounting to 0.6 wt.% Pt.

The specific surface area of pure P25-TiO$_2$ and prepared Pt/P25 catalysts are listed in Table 7. by using single-point N$_2$ physisorption analysis [41, 42]. P25-TiO$_2$ and prepared Pt/P25 had a BET surface area of 47 m^2/g and 46 m^2/g, respectively. It can be clearly observed that the specific surface area of TiO$_2$ did not undergo significant change throughout the deposition of Pt particles process.

Table 7 Pt loading and specific surface area of P25-TiO$_2$ and Pt/P25.

Catalysts	Pt loading (%wt.)	Surface Area (m^2/g)
P25	-	47
Pt/P25	0.58	46

SEM image was used to investigate the morphology of the catalysts [43], as presented in Figure 34 (Appendix F). Similar shapes and size of nanoparticles were observed in pure P25-TiO$_2$ and Pt/P25. Also, EDX spectra were used to investigate the elements on the surface and the EDX results were shown in Figure 35 (Appendix F). The uniform distribution of the elements suggested the uniform dispersion of Pt onto TiO$_2$ supports. Accordingly, the micrographs and spectra confirmed the presence of Pt on P25-TiO$_2$ support even though these were not clearly observed due to the low Pt loading content.

The UV-Vis absorption spectra were used to investigate the light absorption of pure P25-TiO$_2$ and prepared Pt/P25 catalysts and the results were shown in Figure 12. The absorption band of P25-TiO$_2$ was found at 392 nm, which could be ascribed to the

light absorption caused by the excitation of electron transfer from the valence band to the conduction band [21, 24, 44, 45]. Pt/P25 catalyst exhibited two kinds of characteristic light absorption edges in the UV-Vis spectra, including the sharp absorption band in the UV region (wavelength < 400 nm), which was attributed to the band structure of the original P25-TiO$_2$, and the absorption band in the visible spectra (wavelength of 400 – 800 nm), due to the Pt nanoparticles doping [8, 45, 46]. Notably, the absorption tail, that was assigned to the interfacial charge transfer phenomenon between Pt particles and TiO$_2$ support, was less apparent. In addition, the absorption edge of Pt/P25 was located at about 416 nm, indicating that the deposition of Pt onto P25-TiO$_2$ resulted in enhancement of visible light absorption.
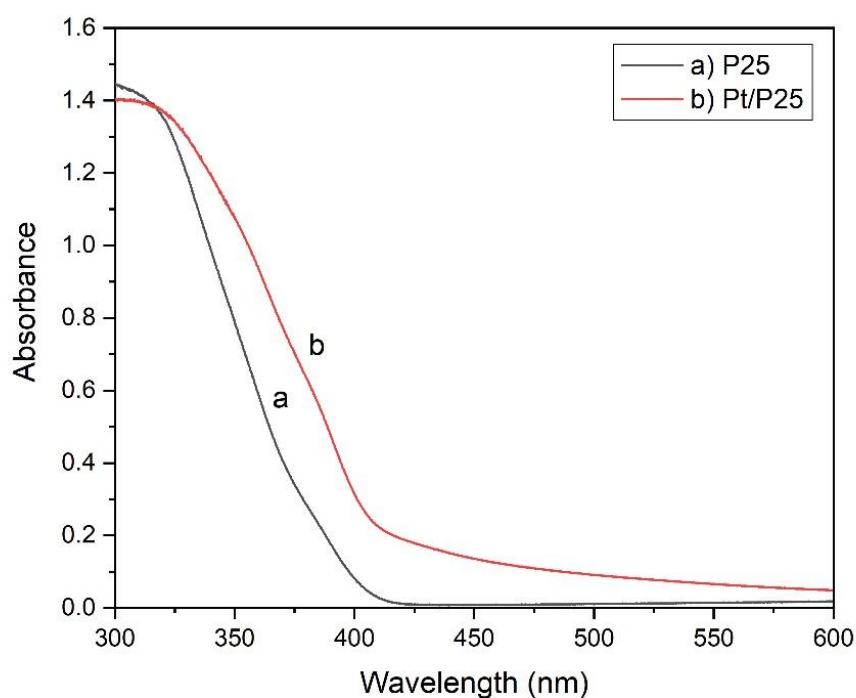
Figure 12 UV–Vis absorbance spectra of (a) pure P25-TiO$_2$ and (b) Pt/P25

The band gap energy of pure and Pt/P25 catalyst was determined by using Tauc relation via the plot of $(h\nu\alpha)^2$ versus photon energy ($h\nu$), as shown in Figure 13. Generally, the band gap energy of pure anatase and rutile phases was 3.2 eV and 3.0 eV, respectively [47]. The band gap energy and the absorption edges of all catalysts were summarized in Table 8. P25-TiO$_2$ had the band gap energy about 3.19 eV, while

Pt/P25 catalyst showed decreased band gap energy. The narrow bandgap resulted in electrons moving from the valence band to the conduction band more easily and quickly than the wider bandgap. It can be concluded that the deposition of Pt onto P25-TiO$_2$ improved the light absorption.
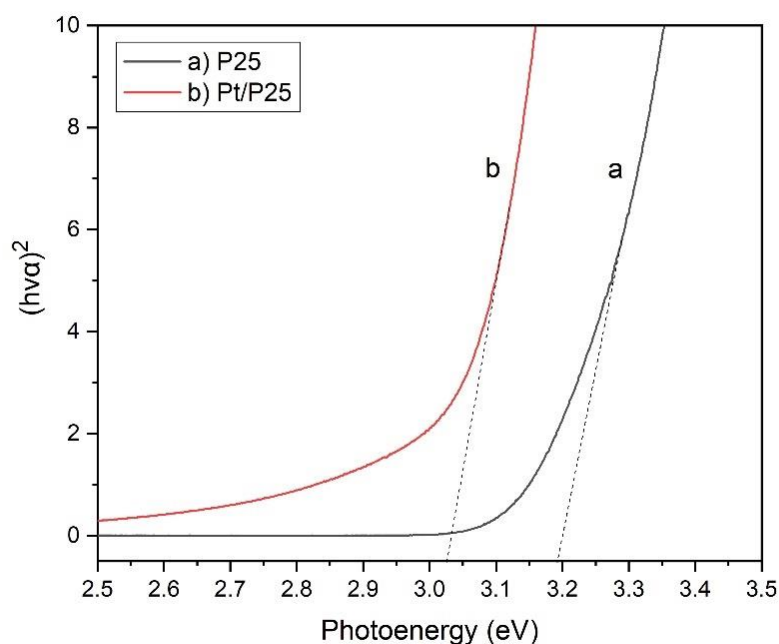
Figure 13 Tauc plot for the band gap calculation of (a) P25-TiO$_2$ and (b) Pt/P25

Table 8 The absorption edges and band gap energy of pure P25-TiO$_2$ and Pt/P25

Catalysts	Wavelength (nm)	Band Gap (eV)
P25	392	3.19
Pt/P25	416	3.03

XPS has been used to investigate the surface composition and chemical states of elements in the catalysts [48, 49]. XPS spectra of P25-TiO$_2$ and Pt/P25 catalysts were deconvoluted and fitted by Gaussian fitting curve. For all the catalysts, the XPS spectra of TiO$_2$ clearly showed the peaks of Ti 2p and O 1s. In the case of Ti 2p, as shown in Figure 14-15, the peaks corresponding to the high-resolution Ti 2p$_{3/2}$ and Ti 2p$_{1/2}$ of TiO$_2$ were located at 458.7 and 464.5 eV, respectively. These peaks were assigned to the

lattice of Ti^{4+} valence state of TiO_2. Meanwhile, two shoulder peaks centered at 457.3 and 463 eV could be assigned to Ti $2p_{3/2}$ and Ti $2p_{1/2}$ of Ti^{3+} valence state, respectively [50-52]. Figure 16-17. exhibited the high-resolution O 1s spectra and two types of surface oxygen species can be identified for P25-TiO_2 and Pt/P25 catalysts. The main and shoulder peaks positioned at 529.9 and 531.8 eV, which were assigned to oxygen species in the TiO_2 lattice (Ti-O) and the hydroxyl groups on the TiO_2 surface (O-H), respectively [40, 53, 54]. The high-resolution Pt 4f XPS spectra of Pt/P25 catalyst was not observed, possibly due to the low Pt doping content. It is notable that the presence of the hydroxyl group in XPS spectra is associated with surface defects and oxygen vacancies. Also, the formation of Ti^{3+} generally related to the formation of surface oxygen vacancies [55]. XPS data analyses results, including the ratio of Ti^{3+}/Ti^{4+} and oxygen vacancy/oxygen lattice of catalysts, were summarized in Table 9. The results suggested that deposited Pt increased the amount of oxygen vacancy on TiO_2, resulting in the greater formation of Ti^{3+}, which may enhance the photocatalytic activity.
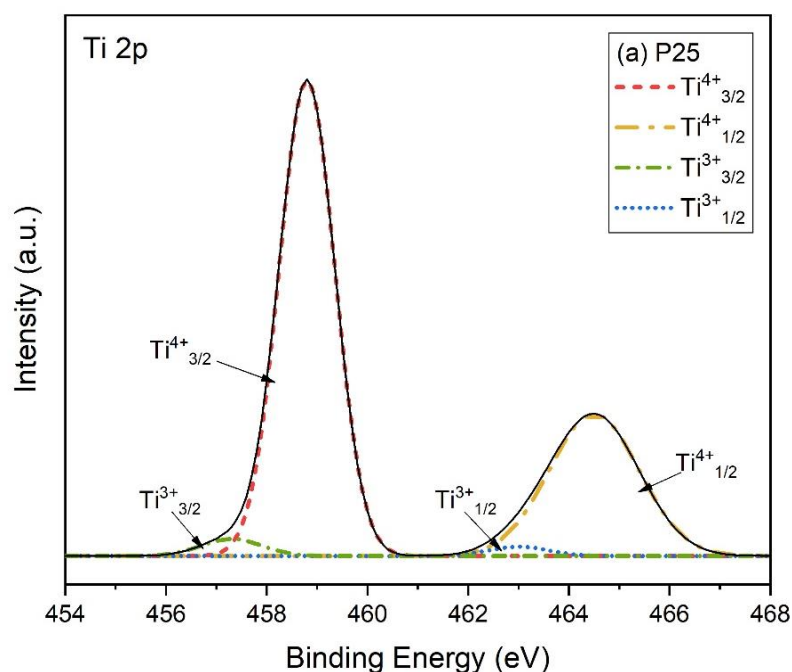
Figure 14 XPS spectra of Ti2p of pure P25-TiO_2 catalyst
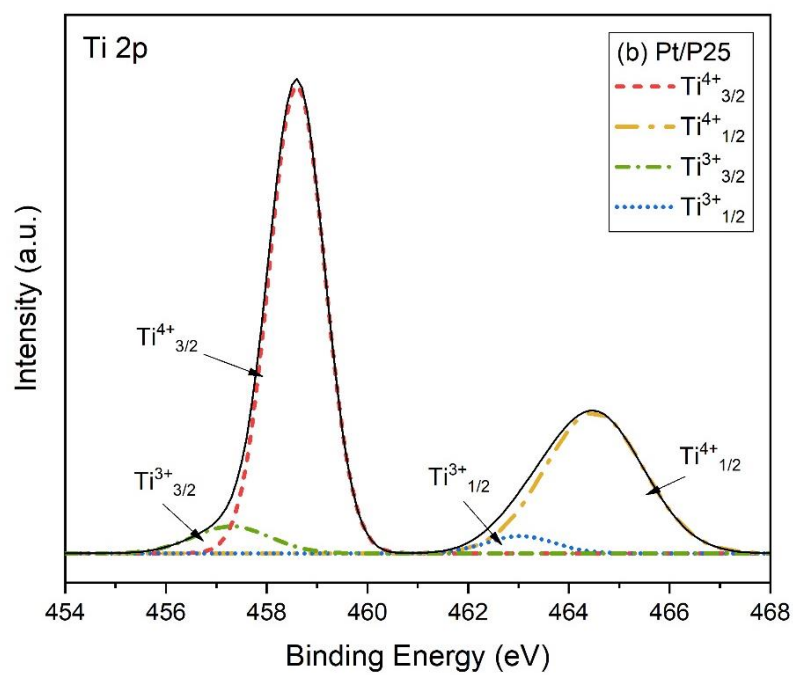
Figure 15 XPS spectra of Ti2p of Pt/P25 catalyst
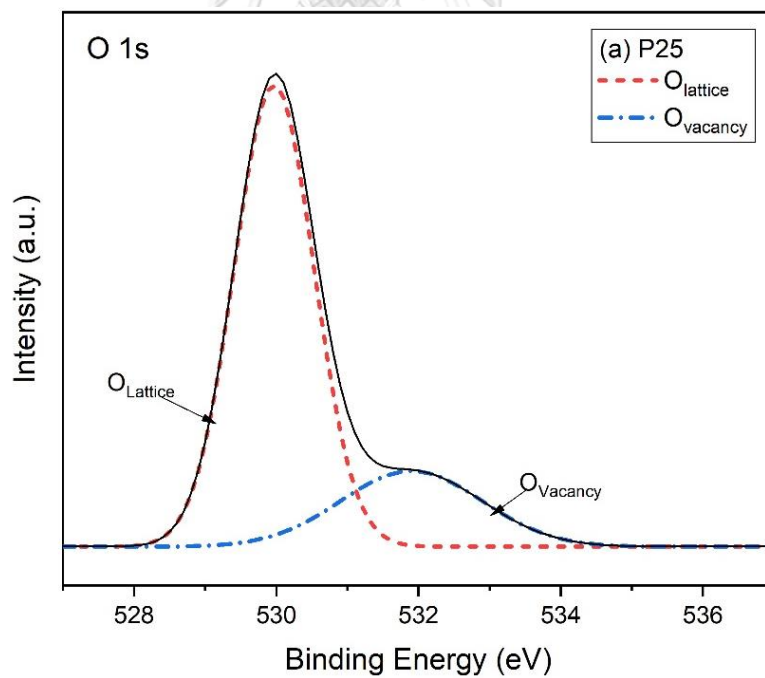
Figure 16 XPS spectra of O1s of pure P25-TiO$_2$ catalyst
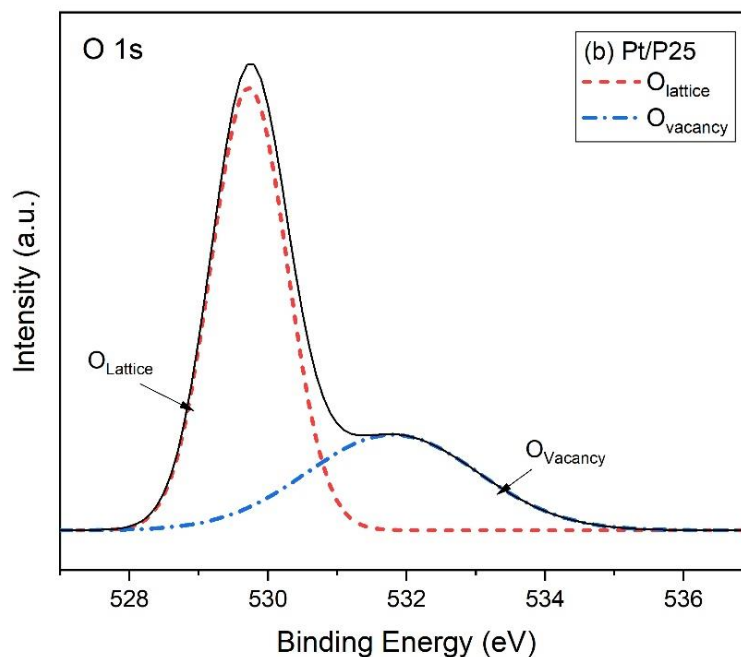
Figure 17 XPS spectra of O1s of Pt/P25 catalyst

Table 9 The ratios of Ti^{3+} to Ti^{4+} and O_v to O_L of catalysts.

Catalysts	Ratio Ti2p Ti^{3+}/Ti^{4+}	Ratio O1s O_v/O_L
P25	0.04	0.29
Pt/P25	0.08	0.49

Photoluminescence spectroscopy (PL) was employed to investigate the efficiency of charge carrier trapping, immigration and transfer of the photogenerated electrons and holes in a photocatalyst [56]. The PL spectra of P25-TiO$_2$ and Pt/P25 catalysts were measured in the wavelength from 375 nm to 550 nm under 325 nm light excitation. As shown in Figure 18, all the catalysts exhibited several PL peaks in the visible region. The band at 404 nm is assigned to the band edge emission which originated from the recombination of photo-excited electron-hole pairs. The peaks at 423, 451, 469, and 484 nm corresponded to a shallow-trap state near absorption band edge emission, corresponded to the presence of oxygen vacancies with two trapped

electrons on TiO$_2$ surface [8, 57-59]. Meanwhile, the peak at 492 nm was assigned to the deep-trap states far below the band edge emissions and collectively called surface state emissions, which corresponded to oxygen vacancy with one electron [8].

In the case of Pt/P25, the PL intensity was decreased as compared to pure P25-TiO$_2$. This could be attributed to the trapping of photoelectron from the conduction band of TiO$_2$ by deposited Pt nanoparticles. This suggested that the deposition of Pt on P25-TiO$_2$ can promote the separation of photogenerated electron and hole effectively and inhibited the electron-hole recombination rate. Consequently, lower electron-hole recombination endowed the Pt/P25 catalyst with high photocatalytic activity.
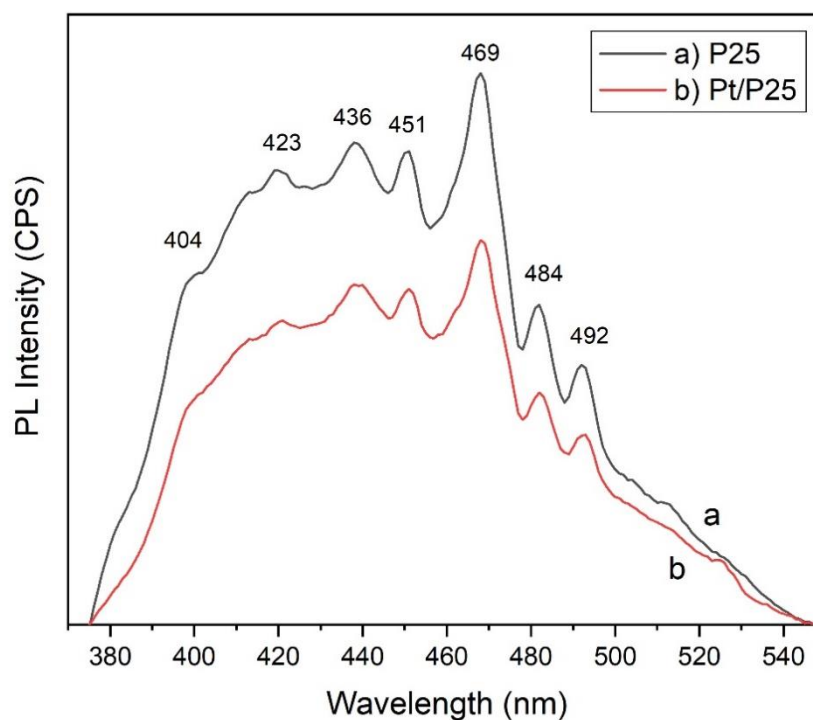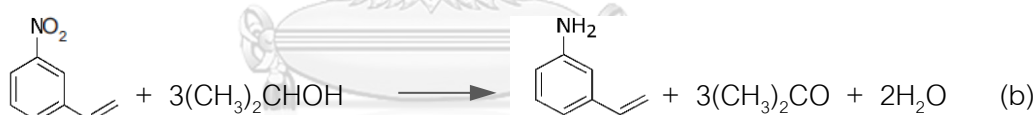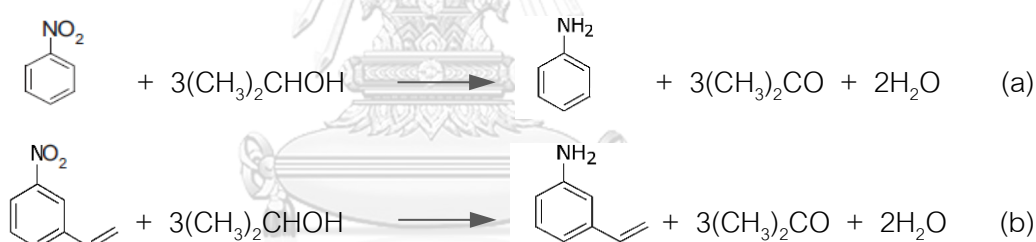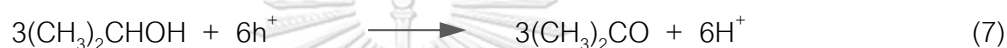

Figure 18 Photoluminescence spectra of (a) pure P25-TiO$_2$ and (b) Pt/P25

4.2 Photocatalytic reaction results

4.2.1 Effect of different nitroaromatics on the photocatalytic performance

The photocatalytic performance of P25-TiO_2 catalyst was evaluated by the selective photocatalytic hydrogenation of different Ar-NO_2, including nitrobenzene (NB) and 3-nitrostyrene (3-NS) in 2-propanol solvent as hydrogen donor under UV light irradiation for 4 h without the use of a reduction gas. The reaction pathways for the photocatalytic hydrogenation of Ar-NO_2 in 2-propanol were shown in Equations (6)-(9) and (a) to (b).

$$TiO_2 + h\nu \longrightarrow h^+ + e^- \tag{6}$$

$$3(CH_3)_2CHOH + 6h^+ \longrightarrow 3(CH_3)_2CO + 6H^+ \tag{7}$$

$$Ar\text{-}NO_2 + 6H^+ + 6e^- \longrightarrow Ar\text{-}NH_2 + 2H_2O \tag{8}$$

$$Ar\text{-}NO_2 + 3(CH_3)_2CHOH \longrightarrow Ar\text{-}NH_2 + 3(CH_3)_2CO + 2H_2O \tag{9}$$

$$+ 3(CH_3)_2CHOH \longrightarrow + 3(CH_3)_2CO + 2H_2O \tag{a}$$

$$+ 3(CH_3)_2CHOH \longrightarrow + 3(CH_3)_2CO + 2H_2O \tag{b}$$
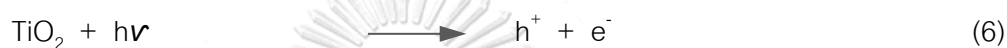
The reaction is initiated by photoexcitation of TiO_2, producing h^+ and e^- pairs, and causing the oxidation and reduction process, respectively. As shown in Figure 19-20, the conversion of Ar-NO_2 was completed after 4 h. Both nitro compounds were quantitively converted into products, which NB was reduced to AN and 3-NS was reduced to 3-VA, with a formation of three equivalents of acetone. This indicated that H atoms of 2-propanol, removed by oxidation with h^+, are consumed quantitively by the -NO_2 to -NH_2 hydrogenation. In addition, H_2 gas was not detected during the reaction, indicating that the H atoms of alcoholic solvents were consumed by oxidation with h^+. However, H_2 can be formed when Ar-NO_2 was almost completely consumed, indicating that reduction of protons (H^+) by e^- also occurred [22, 44, 60, 61].

Interestingly, both NB and 3-NS can produce the corresponding products in greater than 99% selectivity, indicating that only nitro group (N=O) of NB and 3-NS can be reduced by e^{-} and H^{+} to amine group (-NH$_2$) while vinyl group (C=C) of 3-NS was not reduced. In contrast, previous or conventional reaction system led to a mixture of products in which C=C group was reduced to 3-ethylaniline (EA) and 3-ethylnitrobenzene (ENB) [18, 62, 63]. Thus, this photocatalytic system is very effective for the selective hydrogenation of 3-NS to 3-VA, as the desired product, and would be promising for the selective transformations of substrates with other functional groups. Accordingly, it can be concluded that the substrate did not affect the reaction.
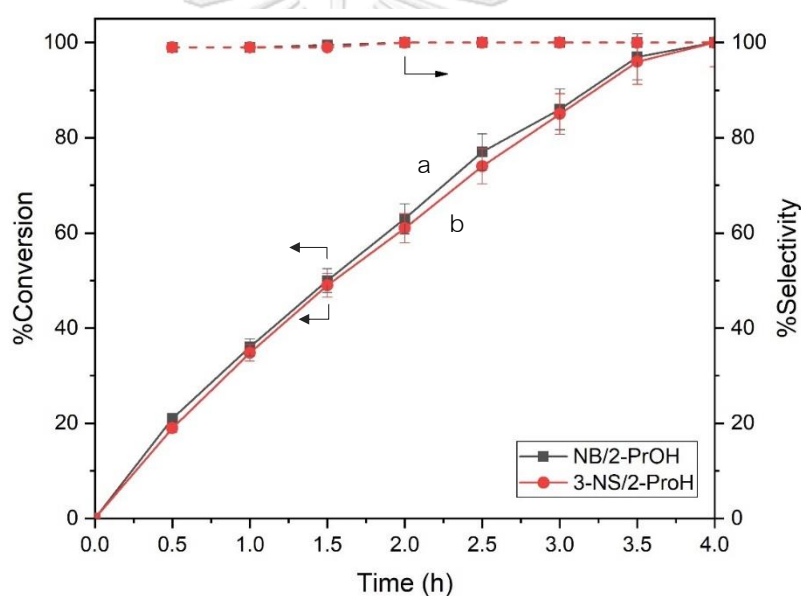

Figure 19 Time-dependent change in %conversion and %selectivity of the hydrogenation of (a) NB and (b) 3-NS in 2-propanol suspension of TiO$_2$ for 4 h.

Figure 20 Time-dependent change in the amounts of reactants and products of the hydrogenation of (a) NB and (b) 3-NS in 2-propanol suspension of TiO_2 for 4 h.

4.2.2 Effect of reactant concentrations on the photocatalytic performance

An extension of the factor of reactants, the photocatalytic activity of the selective photocatalytic hydrogenation of NB in 2-propanol suspension of TiO_2 with different amounts of NB and P25-TiO_2 were presented in Figure 21-23.

As compared to normal amounts of NB substrate and P25-TiO_2 catalyst, the %conversion and the rate of consumed NB were obviously decreased with increasing twice of NB amounts. Meanwhile, increasing the amount of both NB and P25-TiO_2 catalyst was two-fold did not significantly affect to the %conversion and rate of consumed NB. Moreover, the NB conversion slightly decreased with the increase of both NB and P25-TiO_2, probably because the high amount of TiO_2 suppressed the photogeneration of e^- and h^+ by light absorption and the adsorption of the substrate [2]. Also, the time course of products formation is in good agreement with the aforementioned results. Notably, nitrosobenzene (Ar-NO) and phenylhydroxylamine (Ar-NHOH), as intermediates, were not detected, indicating $ArNO_2$ was completely reduced to Ar-NH_2 via Ar-NO and Ar-NHOH formation. This suggested that the photocatalytic conversion of Ar-NO_2 did not depend on the substrate but increased upon increasing

the rates of hydrogen ions (H^+) which related to the rates of acetone formation via the oxidation of 2-propanol by h^+. This indicated that the rate of photocatalytic activity depended on the supply of hydrogen to the catalyst surface for the selective photocatalytic hydrogenation of $Ar-NO_2$. Thus, the proposed reaction mechanism and pathways were shown in Equations (10) to (16).

$$TiO_2 + h\nu \longrightarrow h^+ + e^- \tag{10}$$

$$(CH_3)_2CHOH + 2h^+ \longrightarrow (CH_3)_2CO + 2H^+ \tag{11}$$

$$2H^+ + 2e^- \longrightarrow H_2 \tag{12}$$

$$Ar-NO_2 + 2H^+ + 2e^- \longrightarrow Ar-NO + H_2O \tag{13}$$

$$Ar-NO + 2H^+ + 2e^- \longrightarrow Ar-NHOH \tag{14}$$

$$Ar-NHOH + 2H^+ + 2e^- \longrightarrow Ar-NH_2 + H_2O \tag{15}$$

$$Ar-NO_2 + 3(CH_3)_2CHOH \longrightarrow Ar-NH_2 + 3(CH_3)_2CO + 2H_2O \tag{16}$$

Figure 21 Time-dependent change in %conversion and %selectivity of the hydrogenation of NB in 2-propanol suspension of TiO_2 for 4 h photoirradiation: (a) Normal NB and P25, (b) 2 times of NB, and (c) 2 times of both NB and P25.
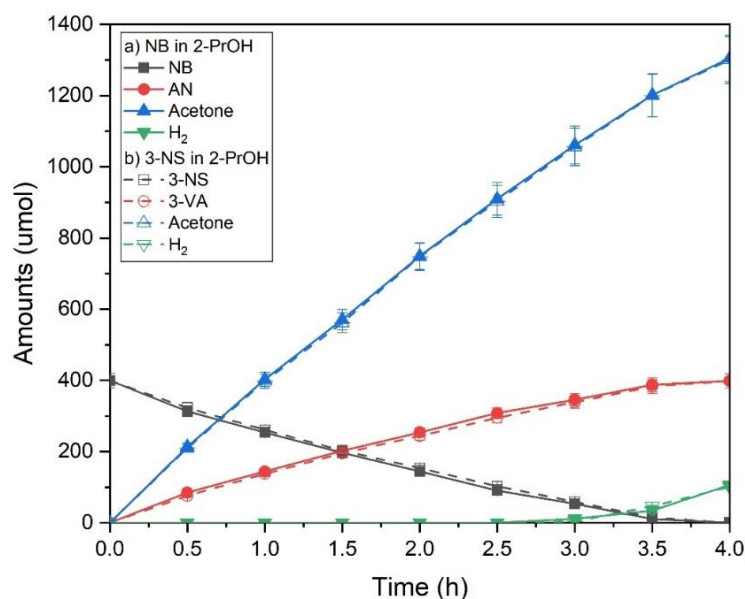
Figure 22 Time-dependent change in the amounts of reactants of the hydrogenation of NB in 2-propanol suspension of TiO_2 for 4 h photoirradiation: (a) Normal NB and P25, (b) 2 times of NB, and (c) 2 times of both NB and P25.
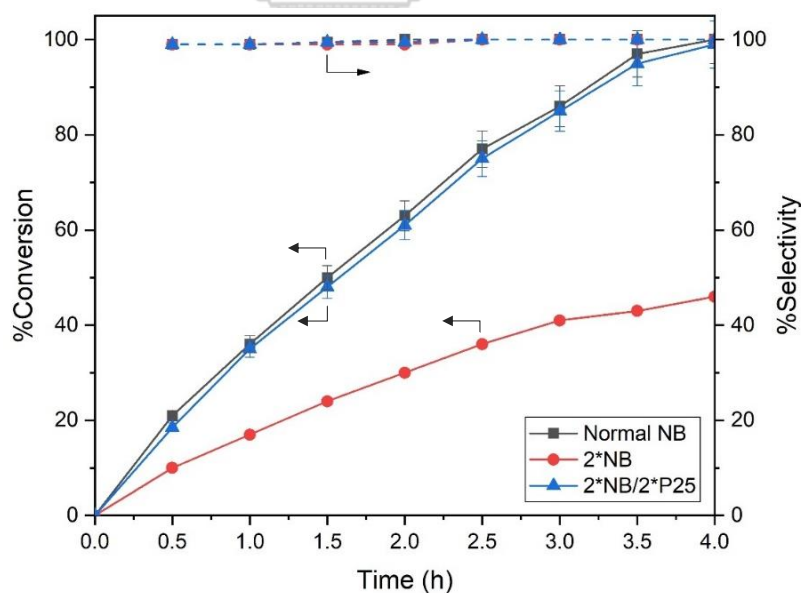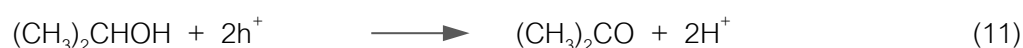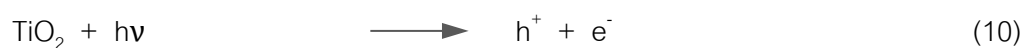

Figure 23 Time-dependent change in the amounts of products of the hydrogenation of NB in 2-propanol suspension of TiO_2 for 4 h photoirradiation: (a) Normal NB and P25, (b) 2 times of NB, and (c) 2 times of both NB and P25.
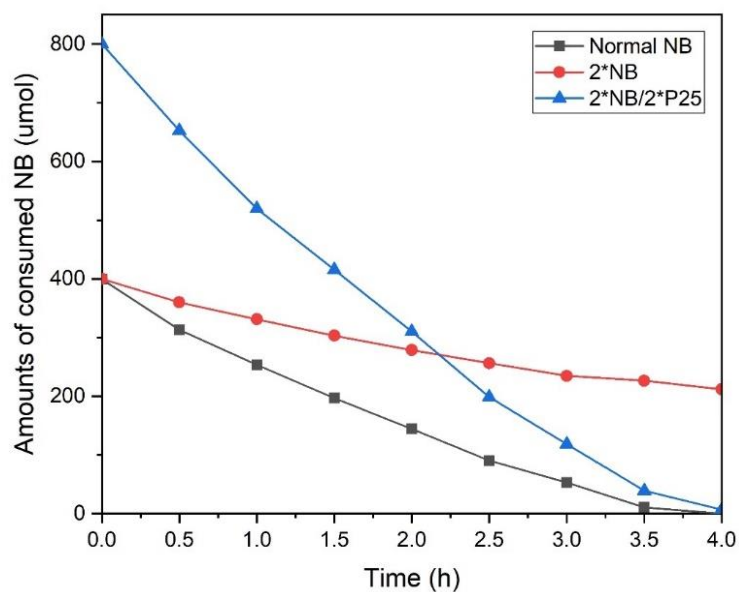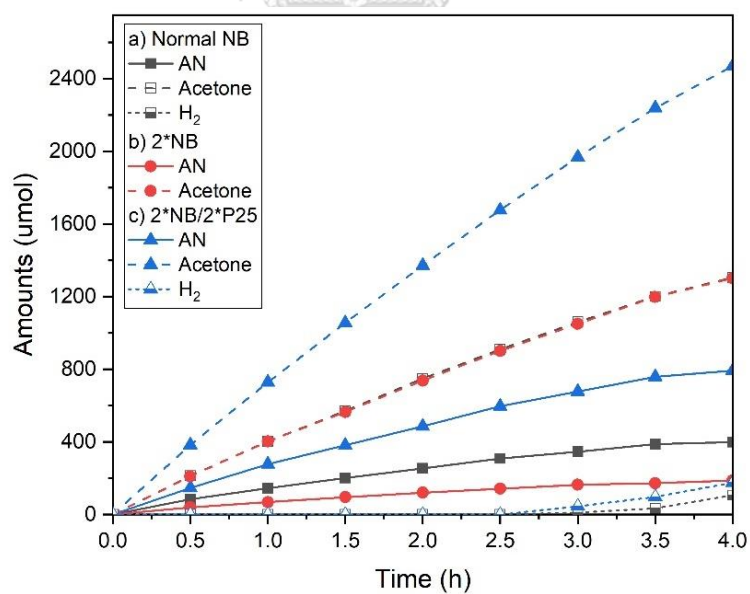
4.2.3 Effect of alcoholic solvents on the photocatalytic performance

Applicability of the selective photocatalytic hydrogenation of NB and 3-NS was investigated using various alcohol solvents, including ethanol, 2-propanol, and butanol, as hydrogen donors. Upon the photoirradiation of P25-TiO$_2$, different products were obtained according to the alcohols. Carbonyl compounds, including acetaldehyde, acetone, and butanone were produced by photocatalytic oxidation of ethanol, 2-propanol, and butanol, respectively. The results showed that the conversion of Ar-NO$_2$ was the highest when ethanol used as a solvent, which resulted from h$^+$ trapping and H$^+$ generation efficiency [22]. It led to the completed reaction faster than the others due to the highest rate of H$^+$ formation by oxidation of ethanol. This was in good agreement with the proposed mechanism, which Equation (11) was the determining step of the reaction. Notably, the selectivity of Ar-NH$_2$ (AN and 3-VA) in alcoholic solvents was reached nearly 100% with completed conversion of Ar-NO$_2$ (NB and 3-NS) except in ethanol solvent, in which the Ar-NH$_2$ selectivity was decreased because by-products, such as imines, can be produced from condensation of the generated acetaldehyde and Ar-NH$_2$ when reaction reached nearly 100% conversion [6, 7, 11], as shown in Equation (17). In contrast, hydrogenation of Ar-NO$_2$ in 2-propanol and butanol solvents did not form any by-products. This accounts for the steric structure of the alcohol as well as the aldehyde [7]. In addition, the photocatalytic performance of P25-TiO$_2$ for the selective photocatalytic hydrogenation of all cases as illustrated in Figure 24-26.

$$Ar\text{-}NH_2 \ + \ R{=}O \longrightarrow Ar\text{-}N{=}R \ + \ H_2O \tag{17}$$
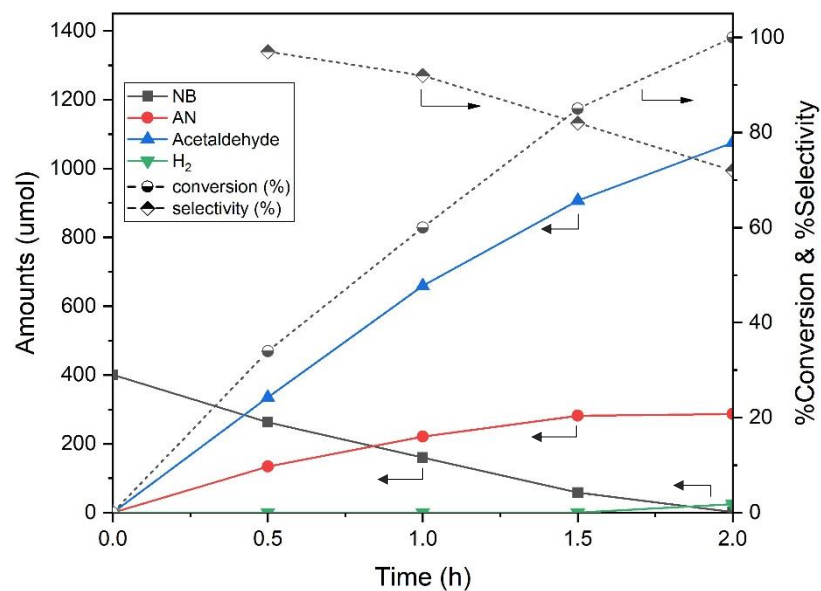
a) NB in EtOH

b) 3-NS in EtOH

Figure 24 Time-dependent change in the conversion, selectivity, and amounts of
reactants and products: (a) NB/ethanol and (b) 3-NS/ethanol using P25-TiO$_2$ for 4 h.

c) NB in 2-PrOH

d) 3-NS in 2-PrOH
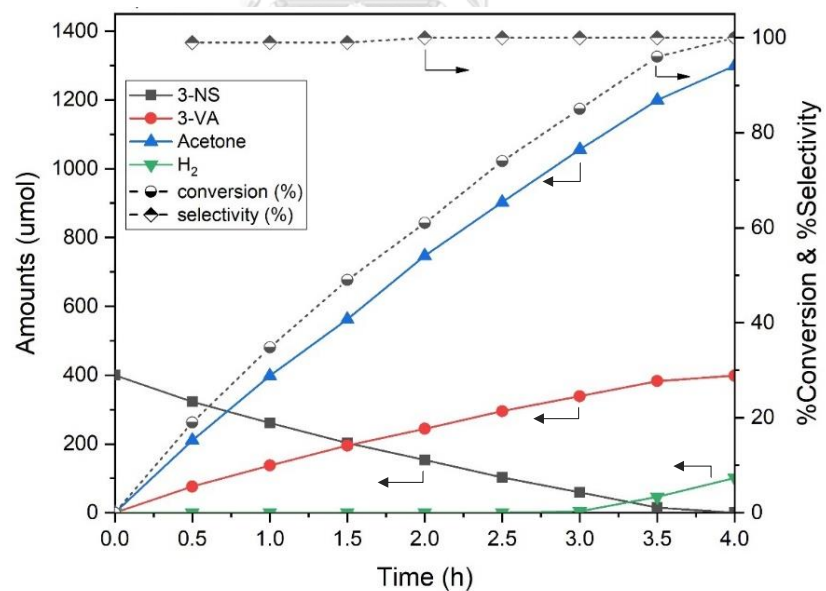
Figure 25 Time-dependent change in the conversion, selectivity, and amounts of reactants and products: (c) NB/2-propanol and (d) 3-NS/2-propanol using P25-TiO$_2$.
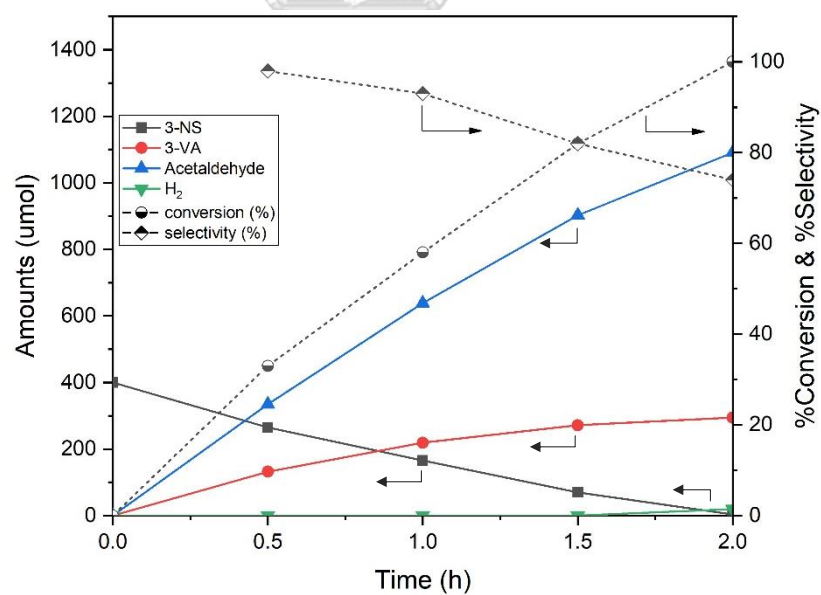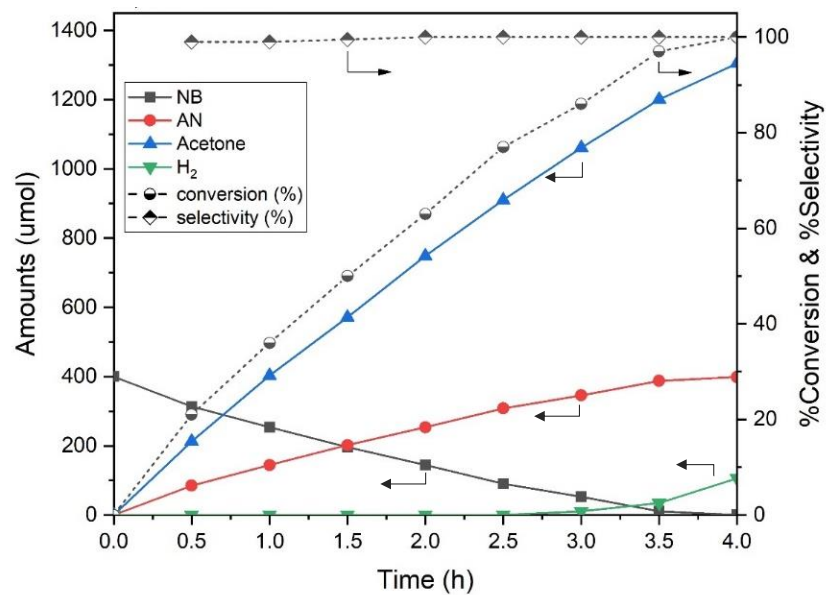
e) NB in BtOH
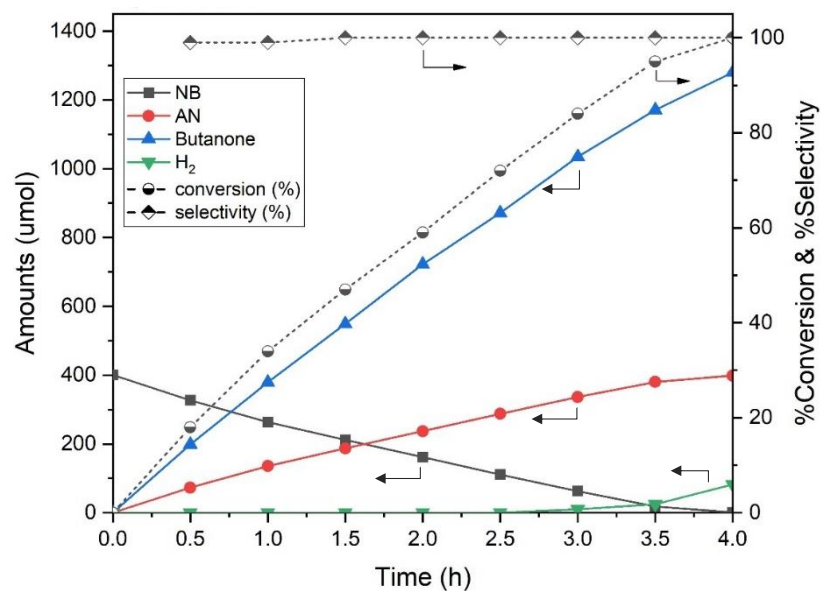
f) 3-NS in BtOH
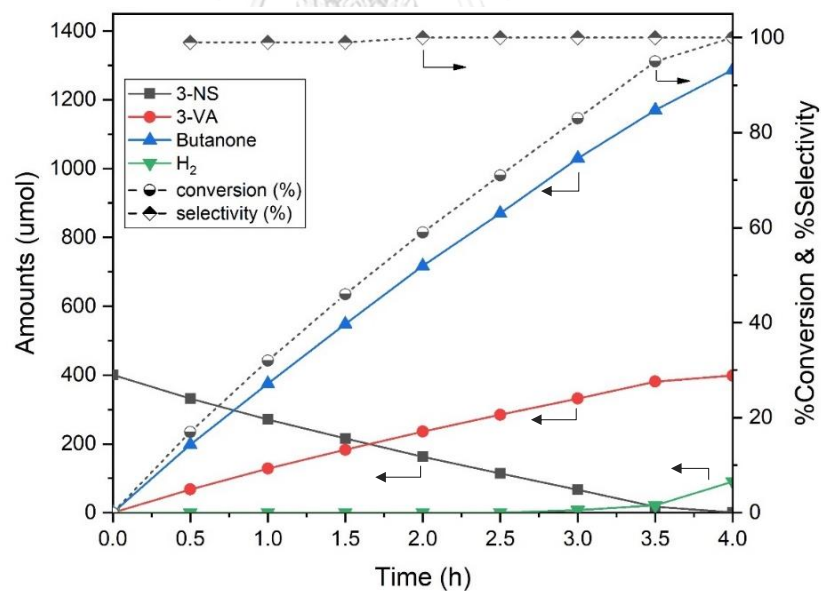
Figure 26 Time-dependent change in the conversion, selectivity, and amounts of reactants and products: (e) NB/butanol and (f) 3-NS/butanol using P25-TiO$_2$ for 4 h.

Furthermore, the photocatalytic performance of P25-TiO$_2$ was examined in various alcohol without adding Ar-NO$_2$ as reactants. It was noted that the amounts of H$_2$ gas formation were remarkably close to the stoichiometric amounts of carbonyl compounds for all alcoholic solvents. This was consistent with the dissociation of alcohol into H$_2$ and carbonyl compounds via reduction and oxidation reactions, respectively [60]. The reaction mechanism was shown in Equations (10) to (12). As shown in Figure 27, the rates of H$_2$ and carbonyl compounds production increased linearly with time, according to a pseudo-zero order rate law, due to the high excess of alcohols [21]. Additionally, ethanol was the best producer of H$_2$ gas and carbonyl compounds, followed by 2-propanol and butanol, which resulted from ethanol trapped h$^+$ and generated H$^+$ more efficiently and produced a larger amount of carbonyl compounds along with H$_2$ gas. The rates of carbonyl compounds and H$_2$ gas formation in all alcohol solvents were summarized in Table 10.
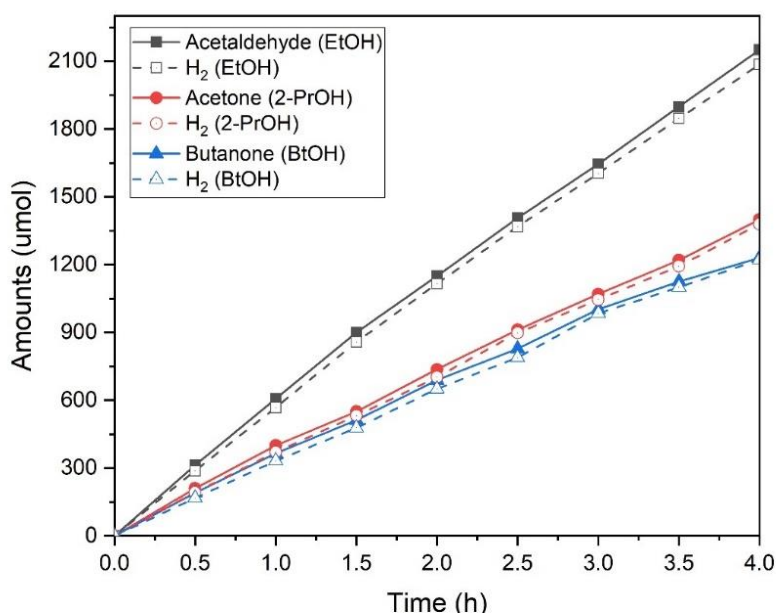
Figure 27 Time-dependent change in the amounts of carbonyl compounds (solid line) and H$_2$ gas (dashed line) in (a) ethanol, (b) 2-propanol, and (c) butanol suspension of TiO$_2$ without reactants for 4 h photoirradiation.

Table   10 Rates of carbonyl compounds and H_2 formation in various alcohol solvents without Ar-NO_2 for 4 h photoirradiation

Alcoholic solvents	Rates of Aldehyde and ketone formation (μmol/h·g$_{cat}$)	Rates of H_2 formation (μmol/h·g$_{cat}$)
Ethanol	2672	2619
2-Propanol	1781	1740
Butanol	1622	1578

According to the photocatalytic performance of catalysts in various alcohol both with and without Ar-NO_2, in which the amounts of Ar-NH_2 production were proportional with the amounts of carbonyl compounds formation at the ratio around 1:3 and H_2 gas can be detected when completed reaction, it can be concluded that the rate of H^+ used for hydrogenation of Ar-NO_2 (Equation (13)) was higher than rate of H^+ formation from alcohol oxidation (Equation (11)).

4.2.4 Effect of Pt/P25-TiO_2 on the photocatalytic performance

There are variously reported regarding the enhancement of catalytic activity and lifetime of the carriers and migration mechanism on the surface of TiO_2 nanoparticles modified by platinum. Thus, the photocatalytic performance of Pt/P25-TiO_2 catalyst was examined in 2-propanol solvent both with and without adding Ar-NO_2 as reactants. In case of no Ar-NO_2, as shown in Figure 28, the photocatalytic performance of Pt/P25 showed that acetone and H_2 gas were produced in molar ratios near the unity and their production rates are considerably larger than those of the P25 catalyst. This due to the migration of photogenerated e^- in CB to the Pt nanoparticles, causing enhancement the charge separation between e^- and h^+ pairs and will, in principle, quicken the oxidation of the 2-propanol by h^+ and the simultaneous reduction of H^+ by e^- [22, 23, 64]. Therefore, the photocatalytic activity increased in general with Pt loading. The rates of acetone and H_2 gas formation of all catalysts were summarized in Table 11.
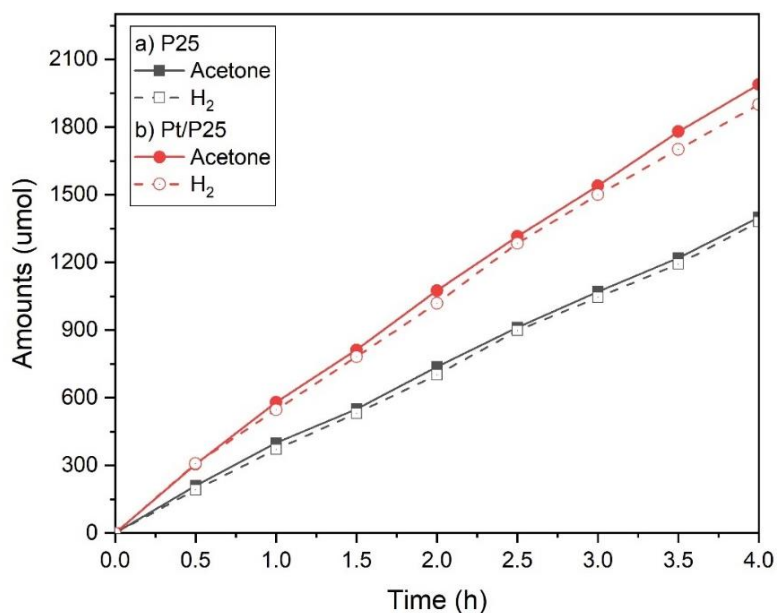
Figure 28 Time-dependent change in the amounts of acetone (solid line) and H_2 gas (dashed line) in 2-propanol suspension of (a) pure P25-TiO$_2$ and (b) Pt/P25 without Ar-NO$_2$ for 4 h photoirradiation.

Table 11 Rates of acetone and H_2 gas formation in 2-propanol solvents without Ar-NO$_2$ substrate for 4 h photoirradiation

Catalysts	Rates of acetone formation (μmol/h·g$_{cat}$)	Rates of H_2 formation (μmol/h·g$_{cat}$)
P25	1781	1740
Pt/TiO$_2$	2568	2489

The photocatalytic performances of Pt/P25 and P25-TiO$_2$ were presented in Figure 29-30. Pt/P25 catalyst showed higher NB conversion as compared with pure P25-TiO$_2$, which the reaction was completed in a shorter time, due to the higher rate of h$^+$ and H$^+$ formations. Also, NB was adsorbed on Pt through partial electron transfer from Pt to Ar-NO$_2$, which e$^-$ in Pt are consumed by the reduction of Ar-NO$_2$ [20, 65]. Thus, the TiO$_2$ supported Pt-based catalyst was very effective for the selective hydrogenation of nitro compounds. This clearly indicated that the high photocatalytic activity in the

presence of Pt/P25 was reasoned in terms of the properties of Pt deposited TiO_2 catalyst, selective adsorption of the substrates, and the charge separation efficiency.

Figure 29 Time-dependent change in the photocatalytic activity of the photocatalytic hydrogenation of NB in 2-propanol suspension of (a) pure P25-TiO_2 and (b) Pt/P25.
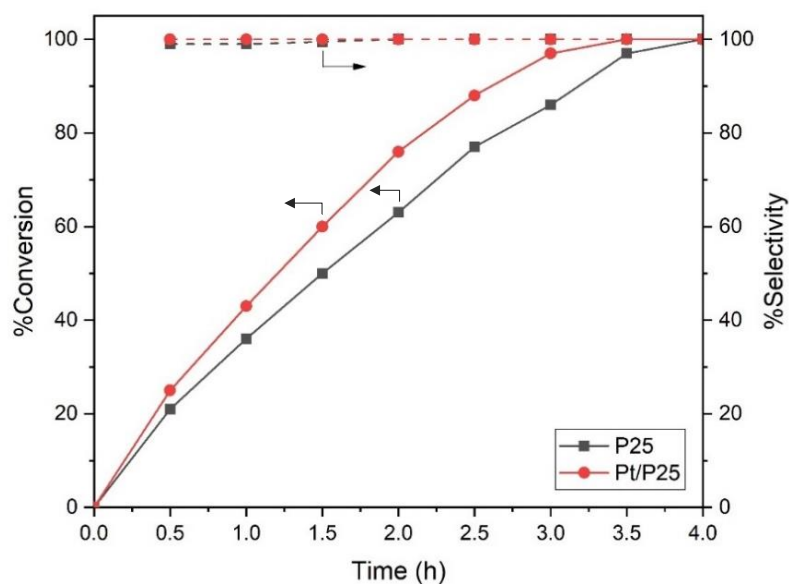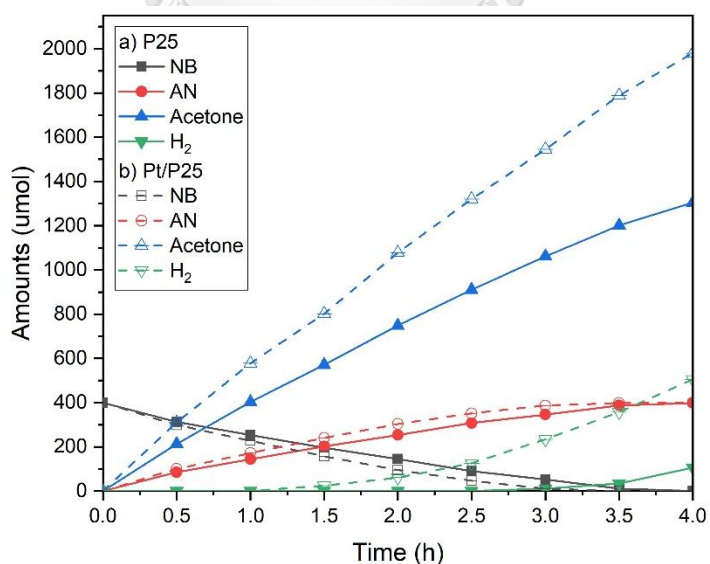

Figure 30 Time-dependent change in the amounts of reactants and products of the hydrogenation of NB in 2-propanol suspension of (a) pure P25-TiO_2 and (b) Pt/P25.

CHAPTER 5
CONCLUSION AND RECOMMENDATION

5.1 Conclusions

The selective photocatalytic hydrogenation of Ar-NO_2 in alcohol solvent under UV light irradiation of P25-TiO_2 catalyst without using reducing gas was a great process because it was safe, which operated at room temperature and atmospheric pressure and can be produced more valuable products. Ar-NO_2 was quantitively reduced by e^- into products, which NB was reduced to AN and 3-NS was reduced to 3-VA, with a production of three equivalents of carbonyl compounds. An increase in the amount of Ar-NO_2 2 times caused the photocatalytic activity decreased. In contrast, adding both the amount of Ar-NO_2 and P25-TiO_2 was twice, the photocatalytic activity did not significantly change. H_2 gas was not detected during the reaction when using Ar-NO_2 as the reactant. Meanwhile, H_2 gas can be detected from the reduction of protons (H^+) by e^- when Ar-NO_2 was absent. Moreover, acetaldehyde, acetone, and butanone were formed by oxidation of ethanol, 2-propanol, and butanol, respectively. Ethanol solvent caused the highest Ar-NO_2 conversion, followed by 2-propanol and butanol. This because ethanol generated H^+ from the oxidation of alcohol the most efficiently. The results were in good agreement with the proposed mechanism. In summary, the selective photocatalytic hydrogenation of Ar-NO_2 did not rely on the substrate but depended on the rate of H^+ formation by the oxidation of alcohol.

For Pt/P25 catalyst, Pt/P25 was successfully synthesized by the conventional impregnation method. The crystalline structure, crystallite size, phase composition, and specific surface area of TiO_2 did not significantly change throughout the deposition of Pt particles process. Also, Pt/P25 catalyst exhibited higher photocatalytic activity than pure P25-TiO_2 support. The deposition of Pt on P25-TiO_2 promoted electron transfer and retarded electron-hole recombination, resulting in higher photocatalytic activity. From the results, it can be concluded that the photocatalytic activity was influenced by hydrogen donor and charge separation efficiency of the catalyst.

5.2 Recommendation

   1. Use other methods to prepare Pt/P25-TiO$_2$ catalyst and compare with conventional impregnation method.

   2. Use other metals to deposit onto TiO$_2$ support and compare with Pt/P25 and P25-TiO$_2$.

   3. Use other substrates to investigate the photocatalytic performance.

REFERENCES

[1]   Imamura, K., T. Yoshikawa, K. Hashimoto and H. Kominami, Stoichiometric production of aminobenzenes and ketones by photocatalytic reduction of nitrobenzenes in secondary alcoholic suspension of titanium(IV) oxide under metal-free conditions. *Applied Catalysis B: Environmental*, 2013. **134-135**: p. 193-197.

[2]   Shiraishi, Y., Y. Togawa, D. Tsukamoto, S. Tanaka and T. Hirai, Highly Efficient and Selective Hydrogenation of Nitroaromatics on Photoactivated Rutile Titanium Dioxide. *ACS Catalysis*, **2012**. **2**(12): p. 2475-2481.

[3]   Kuhaudomlap, S., O. Mekasuwandumrong, P. Praserthdam, S.-I. Fujita, M. Arai and J. Panpranot, The H_2-Treated TiO_2 Supported Pt Catalysts Prepared by Strong Electrostatic Adsorption for Liquid-Phase Selective Hydrogenation. *Catalysts*, **2018**. **8**(2): p. 1-12.

[4]   Berguerand, C., A. Yarulin, F. Cárdenas-Lizana, J. Wärnå, E. Sulman, D.Y. Murzin and L. Kiwi-Minsker, Chemoselective Liquid Phase Hydrogenation of 3-Nitrostyrene over Pt Nanoparticles: Synergy with ZnO Support. *Industrial & Engineering Chemistry Research*, **2015**. **54**(35): p. 8659-8669.

[5]   Song, J., Z.-F. Huang, L. Pan, K. Li, X. Zhang, L. Wang and J.-J. Zou, Review on selective hydrogenation of nitroarene by catalytic, photocatalytic and electrocatalytic reactions. *Applied Catalysis B: Environmental*, 2018. **227**: p. 386-408.

[6]   Tada, H., T. Ishida, A. Takao, S. Ito, S. Mukhopadhyay, T. Akita, K. Tanaka and H. Kobayashi, Kinetic and DFT studies on the Ag/TiO_2-photocatalyzed selective reduction of nitrobenzene to aniline. *Chemphyschem*, **2005**. **6**(8): p. 1537-1543.

[7]   Hakki, A., R. Dillert and D.W. Bahnemann, Factors affecting the selectivity of the photocatalytic conversion of nitroaromatic compounds over TiO_2 to valuable nitrogen-containing organic compounds. *Phys Chem Chem Phys*, **2013**. **15**(8): p. 2992-3002.

[8]   Kaur, J., R. Singh and B. Pal, Influence of coinage and platinum group metal co-

catalysis for the photocatalytic reduction of m-dinitrobenzene by P25 and rutile TiO$_2$. *Journal of Molecular Catalysis A: Chemical*, **2015**. **397**: p. 99-105.

[9]   Torres, C., C. Campos, J.L.G. Fierro, M. Oportus and P. Reyes, Nitrobenzene Hydrogenation on Au/TiO$_2$ and Au/SiO$_2$ Catalyst: Synthesis, Characterization and Catalytic Activity. *Catalysis Letters*, **2013**. **143**(8): p. 763-771.

[10]   Li, X., J. Zhang, Y. Xiang, L. Ma, Q. Zhang, C. Lu, H. Wang and Y. Bai, One pot synthesis of N-ethylaniline from nitrobenzene and ethanol. *Science in China Series B: Chemistry*, **2008**. **51**(3): p. 248-256.

[11]   Flores, S.O., O. Rios-Bernij, M.A. Valenzuela, I. Córdova, R. Gómez and R. Gutiérrez, Photocatalytic reduction of nitrobenzene over titanium dioxide: by-product identification and possible pathways. *Topics in Catalysis*, **2007**. **44**(4): p. 507-511.

[12]   Kohtani, S., E. Yoshioka and H. Miyabe, Photocatalytic Hydrogenation on Semiconductor Particles. *Hydrogenation*, 2012. p. 291-308.

[13]   Imamura, K., S. Iwasaki, T. Maeda, K. Hashimoto, B. Ohtani and H. Kominami, Photocatalytic reduction of nitrobenzenes to aminobenzenes in aqueous suspensions of titanium(IV) oxide in the presence of hole scavengers under deaerated and aerated conditions. *Phys Chem Chem Phys*, 2011. **13**(11): p. 5114-5119.

[14]   Corma, A., P. Serna, P. Concepcion and J.J. Calvino, Transforming nonselective into chemoselective metal catalysts for the hydrogenation of substituted nitroaromatics. *J Am Chem Soc*, **2008**. **130**(27): p. 8748-8753.

[15]   Beier, M.J., J.-M. Andanson and A. Baiker, Tuning the Chemoselective Hydrogenation of Nitrostyrenes Catalyzed by Ionic Liquid-Supported Platinum Nanoparticles. *ACS Catalysis*, **2012**. **2**(12): p. 2587-2595.

[16]   Fujita, S.-i., H. Yoshida, K. Asai, X. Meng and M. Arai, Selective hydrogenation of nitrostyrene to aminostyrene over Pt/TiO$_2$ catalysts: Effects of pressurized carbon dioxide and catalyst preparation conditions. *The Journal of Supercritical Fluids*, **2011**. **60**: p. 106-112.

[17]   Mohamed, M.M. and M.S. Al-Sharif, Visible light assisted reduction of 4-nitrophenol to 4-aminophenol on Ag/TiO$_2$ photocatalysts synthesized by hybrid templates. *Applied Catalysis B: Environmental*, 2013. 142-143: p. 432-441.

[18]   Yoshida, H., N. Igarashi, S.-i. Fujita, J. Panpranot and M. Arai, Influence of Crystallite Size of TiO$_2$ Supports on the Activity of Dispersed Pt Catalysts in Liquid-Phase Selective Hydrogenation of 3-Nitrostyrene, Nitrobenzene, and Styrene. *Catalysis Letters*, 2014. 145(2): p. 606-611.

[19]   Zhang, Y., H. Ma, M. Yi, Z. Shen, X. Yu and X. Zhang, Magnetron-sputtering fabrication of noble metal nanodots coated TiO$_2$ nanoparticles with enhanced photocatalytic performance. *Materials & Design*, 2017. 125: p. 94-99.

[20]   Mahdavi, F., T.C. Bruton and Y. Li, Photoinduced reduction of nitro compounds on semiconductor particles. *The Journal of Organic Chemistry*, 1993. 58(3): p. 744-746.

[21]   Chiarello, G.L., M.H. Aguirre and E. Selli, Hydrogen production by photocatalytic steam reforming of methanol on noble metal-modified TiO$_2$. *Journal of Catalysis*, 2010. 273(2): p. 182-190.

[22]   López, C.R., E.P. Melián, J.A. Ortega Méndez, D.E. Santiago, J.M. Doña Rodríguez and O. González Díaz, Comparative study of alcohols as sacrificial agents in H$_2$ production by heterogeneous photocatalysis using Pt/TiO$_2$ catalysts. *Journal of Photochemistry and Photobiology A: Chemistry*, 2015. 312: p. 45-54.

[23]   Sun, B., A.V. Vorontsov and P.G. Smirniotis, Role of Platinum Deposited on TiO$_2$ in Phenol Photocatalytic Oxidation. *Langmuir*, 2003. 19(8): p. 3151-3156.

[24]   Jiang, Z., J. Li, W. Liao, G. Fan, H. Yu, L. Chen and Z. Su, Synthesis and Characterization of the Optical Properties of Pt-TiO$_2$ Nanotubes. *Journal of Nanomaterials*, 2017. 2017: p. 1-9.

[25]   Fang, W., M. Xing and J. Zhang, Modifications on reduced titanium dioxide photocatalysts: A review. *Journal of Photochemistry and Photobiology C: Photochemistry Reviews*, 2017. 32: p. 21-39.

[26]   Fujishima, A., X. Zhang and D. Tryk, TiO$_2$ photocatalysis and related surface

phenomena. *Surface Science Reports*, **2008**. **63**(12): p. 515-582.

[27] Regonini, D., C.R. Bowen, A. Jaroenworaluck and R. Stevens, A review of growth mechanism, structure and crystallinity of anodized TiO_2 nanotubes. *Materials Science and Engineering: R: Reports*, **2013**. **74**(12): p. 377-406.

[28] Ohtani, B., O.O. Prieto-Mahaney, D. Li and R. Abe, What is Degussa (Evonik) P25? Crystalline composition analysis, reconstruction from isolated pure particles and photocatalytic activity test. *Journal of Photochemistry and Photobiology A: Chemistry*, **2010**. **216**(2-3): p. 179-182.

[29] Ohno, T., K. Sarukawa, K. Tokieda and M. Matsumura, Morphology of a TiO_2 Photocatalyst (Degussa, P-25) Consisting of Anatase and Rutile Crystalline Phases. *Journal of Catalysis*, **2001**. **203**(1): p. 82-86.

[30] Serna, P. and A. Corma, Transforming Nano Metal Nonselective Particulates into Chemoselective Catalysts for Hydrogenation of Substituted Nitrobenzenes. *ACS Catalysis*, **2015**. **5**(12): p. 7114-7121.

[31] Pisduangdaw, S., O. Mekasuwandumrong, S.-I. Fujita, M. Arai, H. Yoshida and J. Panpranot, One step synthesis of Pt–Co/TiO_2 catalysts by flame spray pyrolysis for the hydrogenation of 3-nitrostyrene. *Catalysis Communications*, **2015**. **61**: p. 11-15.

[32] Serna, P., P. Concepción and A. Corma, Design of highly active and chemoselective bimetallic gold–platinum hydrogenation catalysts through kinetic and isotopic studies. *Journal of Catalysis*, **2009**. **265**(1): p. 19-25.

[33] Han, X., R. Zhou, G. Lai and X. Zheng, Influence of support and transition metal (Cr, Mn, Fe, Co, Ni and Cu) on the hydrogenation of p-chloronitrobenzene over supported platinum catalysts. *Catalysis Today*, **2004**. **93-95**: p. 433-437.

[34] Boonstra, A.H. and C.A.H.A. Mutsaers, Photohydrogenation of ethyne and ethene on the surface of titanium dioxide. *The Journal of Physical Chemistry*, **1975**. **79**(19): p. 2025-2027.

[35] Liqiang, J., Q. Yichun, W. Baiqi, L. Shudan, J. Baojiang, Y. Libin, F. Wei, F. Honggang and S. Jiazhong, Review of photoluminescence performance of nano-sized semiconductor materials and its relationships with photocatalytic activity.

Solar Energy Materials and Solar Cells, **2006**. **90**(12): p. 1773-1787.

[36]   Aditya, T., A. Pal and T. Pal, Nitroarene reduction: a trusted model reaction to test nanoparticle catalysts. **2015**. **51**(46): p. 9410-9431.

[37]   Yoshihiko Ohama and D.V. Gemert, Application of Titanium Dioxide Photocatalysis to Construction Materials. *State-of-the-Art Report of the RILEM Technical Committee 194-TDP*, **2011**.

[38]   Higashimoto, S., Y. Nakai, M. Azuma, M. Takahashi and Y. Sakata, One-pot synthesis of imine from benzyl alcohol and nitrobenzene on visible-light responsive CdS–TiO$_2$ photocatalysts. *RSC Adv.*, **2014**. **4**(71): p. 37662-37668.

[39]   Aghaei, P. and R.J. Berger, Reaction kinetics investigation of the selective oxidation of aqueous ethanol solutions with air over a Au/TiO$_2$ catalyst. *Applied Catalysis B: Environmental*, **2013**. **132-133**: p. 195-203.

[40]   Papavasiliou, J., A. Paxinou, G. Sowik, S. Neophytides and G. Avgouropoulos, Steam Reforming of Methanol over Nanostructured Pt/TiO$_2$ and Pt/CeO$_2$ Catalysts for Fuel Cell Applications. *Catalysts*, **2018**. **8**(11).

[41]   Chen, M., Y. Ma, Y. Zhou, C. Liu, Y. Qin, Y. Fang, G. Guan, X. Li, Z. Zhang and T. Wang, Influence of Transition Metal on the Hydrogen Evolution Reaction over Nano-Molybdenum-Carbide Catalyst. *Catalysts*, **2018**. **8**(7).

[42]   Liu, B., L.-M. Liu, X.-F. Lang, H.-Y. Wang, X.W. Lou and E.S. Aydil, Doping high-surface-area mesoporous TiO$_2$ microspheres with carbonate for visible light hydrogen production. *Energy & Environmental Science*, **2014**. **7**(8).

[43]   Annamalai Leelavathi, T.U.B.R., Thalappil Pradeep, Supported quantum clusters of silver as enhanced catalysts for reduction. *Nanoscale Research Letters,* **2011**. **6**(123).

[44]   Ahmad, H., S.K. Kamarudin, L.J. Minggu and M. Kassim, Hydrogen from photo-catalytic water splitting process: A review. *Renewable and Sustainable Energy Reviews*, **2015**. **43**: p. 599-610.

[45]   Kočí, K., K. Matějů, L. Obalová, S. Krejčíková, Z. Lacný, D. Plachá, L. Čapek, A. Hospodková and O. Šolcová, Effect of silver doping on the TiO$_2$ for photocatalytic

reduction of CO_2. *Applied Catalysis B: Environmental*, **2010**. **96**(3-4): p. 239-244.

[46]   Hirakawa, H., M. Katayama, Y. Shiraishi, H. Sakamoto, K. Wang, B. Ohtani, S. Ichikawa, S. Tanaka and T. Hirai, One-pot synthesis of imines from nitroaromatics and alcohols by tandem photocatalytic and catalytic reactions on Degussa (Evonik) P25 titanium dioxide. *ACS Appl Mater Interfaces*, **2015**. **7**(6): p. 3797-806.

[47]   Ji, Y., L. Zhou, C. Ferronato, X. Yang, A. Salvador, C. Zeng and J.-M. Chovelon, Photocatalytic degradation of atenolol in aqueous titanium dioxide suspensions: Kinetics, intermediates and degradation pathways. *Journal of Photochemistry and Photobiology A: Chemistry*, **2013**. **254**: p. 35-44.

[48]   Ratova, M., R. Klaysri, P. Praserthdam and P.J. Kelly, Visible light active photocatalytic C-doped titanium dioxide films deposited via reactive pulsed DC magnetron co-sputtering: Properties and photocatalytic activity. *Vacuum*, **2018**. **149**: p. 214-224.

[49]   Carrus, M., M. Fantauzzi, F. Riboni, M. Makosch, A. Rossi, E. Selli and J.A. van Bokhoven, Increased conversion and selectivity of 4-nitrostyrene hydrogenation to 4-aminostyrene on Pt nanoparticles supported on titanium-tungsten mixed oxides. *Applied Catalysis A: General*, **2016**. **519**: p. 130-138.

[50]   Jun, J., M. Dhayal, J.-H. Shin, J.-C. Kim and N. Getoff, Surface properties and photoactivity of TiO_2 treated with electron beam. *Radiation Physics and Chemistry*, **2006**. **75**(5): p. 583-589.

[51]   Şen, F. and G. Gökağaç, Different Sized Platinum Nanoparticles Supported on Carbon: An XPS Study on These Methanol Oxidation Catalysts. *The Journal of Physical Chemistry C*, **2007**. **111**(15): p. 5715-5720.

[52]   Xiong, Z., Z. Lei, C.-C. Kuang, X. Chen, B. Gong, Y. Zhao, J. Zhang, C. Zheng and J.C.S. Wu, Selective photocatalytic reduction of CO_2 into CH_4 over Pt-Cu_2O TiO_2 nanocrystals: The interaction between Pt and Cu_2O cocatalysts. *Applied Catalysis B: Environmental*, **2017**. **202**: p. 695-703.

[53]   Zuo, F., L. Wang, T. Wu, Z. Zhang, D. Borchardt and P. Feng, Self-doped Ti^{3+} enhanced photocatalyst for hydrogen production under visible light. *J Am Chem*

Soc, 2010. **132**(34): p. 11856-11857.

[54]   He, M., J. Ji, B. Liu and H. Huang, Reduced TiO_2 with tunable oxygen vacancies for catalytic oxidation of formaldehyde at room temperature. *Applied Surface Science*, 2019. **473**: p. 934-942.

[55]   Jiang, X., Y. Zhang, J. Jiang, Y. Rong, Y. Wang, Y. Wu and C. Pan, Characterization of Oxygen Vacancy Associates within Hydrogenated TiO_2: A Positron Annihilation Study. *The Journal of Physical Chemistry C*, 2012. **116**(42): p. 22619-22624.

[56]   Yan, J., G. Wu, N. Guan, L. Li, Z. Li and X. Cao, Understanding the effect of surface/bulk defects on the photocatalytic activity of TiO_2: anatase versus rutile. *Phys Chem Chem Phys*, 2013. **15**(26): p. 10978-10988.

[57]   Jiang, Y., Z. Yang, P. Zhang, H. Jin and Y. Ding, Natural assembly of a ternary Ag–SnS–TiO_2 photocatalyst and its photocatalytic performance under simulated sunlight. *RSC Advances*, 2018. **8**(24): p. 13408-13416.

[58]   Li, H., Z. Bian, J. Zhu, Y. Huo, H. Li and Y. Lu, Mesoporous Au/TiO_2 nanocomposites with enhanced photocatalytic activity. *J Am Chem Soc*, 2007. **129**(15): p. 4538-4539.

[59]   Tahir, M. and N.S. Amin, Indium-doped TiO_2 nanoparticles for photocatalytic CO_2 reduction with H_2O vapors to CH_4. *Applied Catalysis B: Environmental*, 2015. **162**: p. 98-109.

[60]   Puga, A.V., A. Forneli, H. García and A. Corma, Production of H_2 by Ethanol Photoreforming on Au/TiO_2. *Advanced Functional Materials*, 2014. **24**(2): p. 241-248.

[61]   Tentu, R.D. and S. Basu, Photocatalytic water splitting for hydrogen production. *Current Opinion in Electrochemistry*, 2017. **5**(1): p. 56-62.

[62]   Mitsudome, T., Y. Mikami, M. Matoba, T. Mizugaki, K. Jitsukawa and K. Kaneda, Design of a silver-cerium dioxide core-shell nanocomposite catalyst for chemoselective reduction reactions. *Angew Chem Int Ed Engl*, 2012. **51**(1): p. 136-139.

[63]   Bernard Cog, A.T., R. Dutartre and F. Figueras, Influence of support and metallic precursor on the hydrogenation of p-chloronitrobenzene over supported platinum catalysts. *Journal of Molecular Catalysis*, **1993**. **79**: p. 253-264.

[64]   Ma, Y., Q. Xu, X. Zong, D. Wang, G. Wu, X. Wang and C. Li, Photocatalytic H_2 production on $Pt/TiO_2–SO_4^{2-}$ with tuned surface-phase structures: enhancing activity and reducing CO formation. *Energy Environ. Sci.*, **2012**. **5**(4): p. 6345-6351.

[65]   Kominami, H., S. Yamamoto, K. Imamura, A. Tanaka and K. Hashimoto, Photocatalytic chemoselective reduction of epoxides to alkenes along with formation of ketones in alcoholic suspensions of silver-loaded titanium(iv) oxide at room temperature without the use of reducing gases. *Chem Commun (Camb)*, **2014**. **50**(35): p. 4558-4560.
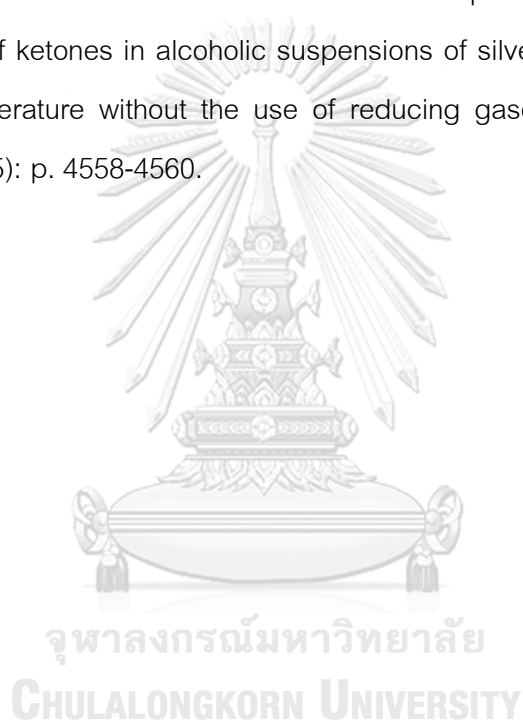
APPENDICES

APPENDIX A

LIGHTING INSTRUMENT AND THE PHOTOCATALYTIC REACTOR

The bulbs were used as a light source for the photocatalytic hydrogenation reaction. The properties of the bulb were listed in Table 12.

Table 12 The properties of the light bulbs

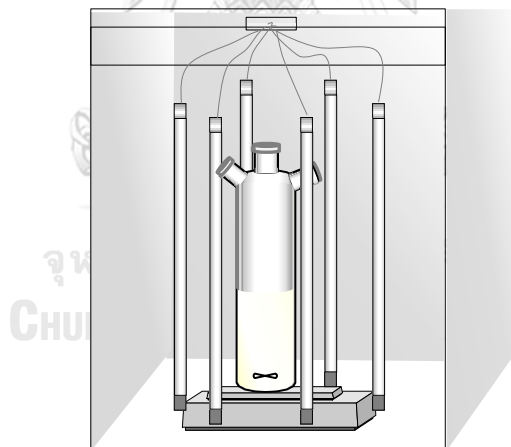| Type of light	UVC light
Brand	Philip
Power (W)	16
Number of bulbs	6
Wavelength (nm)	200-280

Figure 31 Schematic diagram of the photocatalytic hydrogenation set

APPENDIX B

CALCULATION OF THE CRYSTALLITE SIZE

Calculation of the crystallite size by Debye-Scherrer equation

The crystallite size of TiO_2 was calculated from XRD pattern results according to FWHM by the Debye-Scherrer equation (Equations (18)) that was suitable for particle size below 100 nm.

Debye-Scherer equation:

$$D = \frac{k\lambda}{\beta cos\theta} \tag{18}$$

Where

D = Crystallite size (Å)

k = Crystallite-shape factor (0.9)

λ = X-ray wavelength (1.5418 Å for CuK_α)

β = X-ray diffraction broadening (radian)

θ = Observed peak angel (degree)

The X-ray diffraction broadening (β) can be obtained by using Warren's formula (Equation (19)).

Warren's equation:

$$\beta^2 = \beta_M^2 - \beta_S^2$$

$$\beta = \sqrt{\beta_M^2 - \beta_S^2} \tag{19}$$

Where

β_M = Measured peak width in radians at half peak height

β_S = Corresponding width of a standard material

Example: Calculation of the crystallite site of P25-TiO$_2$.

Finding the half-weight width (101) diffraction peak at 25.3° from the XRD pattern.

The half-weight width (101) diffraction peak;

$$\beta_M = 0.3959 \quad \text{degree}$$

$$\beta_M = 0.0069 \quad \text{radian}$$

The corresponding half-height width of the peak of P25-TiO$_2$

$$\beta_S = 0.003836 \quad \text{radian}$$

The pure width

$$\beta = \sqrt{\beta_M^2 - \beta_S^2}$$

$$\beta = \sqrt{0.0069^2 - 0.0038^2}$$

$$\beta = 0.00575 \quad \text{radian}$$

Where

λ	=	1.54	Å
β	=	0.00575	radian
2θ	=	25.3	degree
θ	=	12.65	degree

The crystallite size:

$$D = \frac{k\lambda}{\beta\cos\theta}$$

$$= \frac{(0.9)(1.54)}{(0.00575)\cos(12.65)}$$

$$= 241.89 \quad \text{Å}$$

$$= 24.19 \quad \text{nm}$$

APPENDIX C

CALCULATION OF WEIGHT COMPOSITION

The weight fraction of P25-TiO$_2$ was calculated from the XRD pattern, as shown in Equations (20) to (22).

$$W_A = \frac{K_A A_A}{K_A A_A + K_B A_B + K_R} \tag{20}$$

$$W_B = \frac{K_B A_B}{K_A A_A + K_B A_B + K_R} \tag{21}$$

$$W_R = \frac{K_R}{K_A A_A + K_B A_B + K_R} \tag{22}$$

Where

W_A	=	Weight fraction of anatase phase TiO$_2$
W_B	=	Weight fraction of brookite phase TiO$_2$
W_R	=	Weight fraction of rutile phase TiO$_2$
A_A	=	The intensity of anatase peak
A_B	=	The intensity of brookite peak
A_R	=	The intensity of rutile peak
K_A	=	The coefficient factor of anatase (0.886)
K_B	=	The coefficient factor of brookite (2.721)

The phases of TiO$_2$ can be calculated from the integrated intensities of the peak at $2\theta = 25.3°$ (anatase phase), the peak at $27.4°$ (rutile phase), and the peak at $30.6°$ (brookite phase). However, P25-TiO$_2$ catalyst consisted of anatase phase and rutile phase except for brookite phase.

Example: Calculation of the phase composition of P25-TiO$_2$.

Where

The integrated intensities of anatase (A$_A$)　　=　　2297.4

The integrated intensities of rutile (A$_R$)　　=　　449.3

The weight fraction of the phase content can be calculated by as follows:

$$W_A = \frac{2297.4(0.886)}{2297.4(0.886) + 449.3} = 0.82$$

$$W_R = \frac{449.3}{2297.4(0.886) + 449.3} = 0.18$$

จุฬาลงกรณ์มหาวิทยาลัย

CHULALONGKORN UNIVERSITY

APPENDIX D

CALCULATION OF THE BAND GAP ENERGY FROM UV-VIS SPECTRA

The band gap energy of TiO_2 and modified TiO_2 can be determined from UV-Vis spectra by plotting $(\alpha h\nu)^{\frac{1}{n}}$ versus photon energy ($h\nu$). The photon energy ($h\nu$) and optical absorption coefficient (α) were estimated by Equations (23) to (25).

$$h\nu = E_g = \frac{hc}{\lambda} \tag{23}$$

$$h\nu = \frac{1240}{\lambda} \tag{24}$$

Where

E_g	=	Band gap energy of catalyst (eV)
h	=	Plank constant (6.62×10^{-34} Joules·sec)
c	=	Speed of light (3.0×10^8 meter/sec)
λ	=	Wavelength from UV-vis spectra (nm)

Note: 1 eV is 1.6×10^{-19} Joules

$$\alpha = \frac{2.303A}{t} \tag{25}$$

Where

α	=	Optical absorption coefficient
A	=	Absorbance
t	=	Thickness of the sample

Example: Calculation of the band gap energy of P25-TiO$_2$

To determine the band gap energy of P25-TiO$_2$, the power factor (n) was 0.5 due to the direct band gap finding.
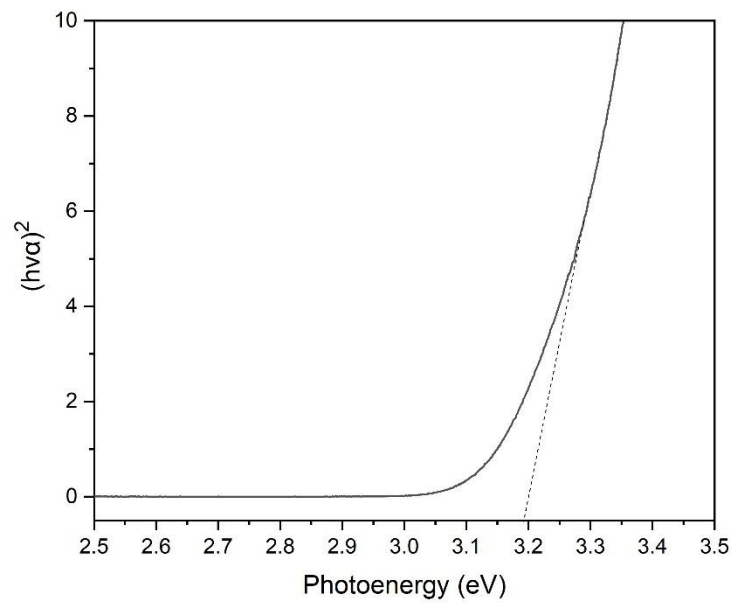

Figure 32 A plot between $(\alpha h\nu)^{(1/0.5)}$ vs. photon energy (hν) of P25-TiO$_2$

From Figure 33, the straight-line cut the X-axis presented the band gap energy of pure P25-TiO$_2$ is 3.19 eV.

APPENDIX E

CALCULATION OF PLATINUM CONTENT ON TITANIA FROM ICP-AES

The loading contents of Pt deposited on P25-TiO_2 support were calculated from ICP-AES results.

For 0.6 wt%. Pt/P25, the initial weight of catalyst powder was 0.05 g.

For 1.0 g of catalyst, Pt contents = 0.006 g

For 0.05 g of catalyst, Pt contents $= \dfrac{0.006 \times 0.05}{1.0}$ g

$= 0.3 \times 10^{-3}$ g = 0.3 mg

For digestion, sample was diluted to obtain 100 cm^3.

Thus, the concentration of sample $= \dfrac{0.3 \times 1000}{100}$ ppm

= 3.0 ppm (mg/L of Pt)

From the result of ICP-AES, the concentration of sample = 2.89 ppm.

The Pt contents deposited P25-TiO_2 were calculated:

Pt loading content $= \dfrac{2.89 \times 0.6}{3.0}$

= 0.58 wt.% Pt/P25-TiO_2

APPENDIX F

SEM IMAGES AND EDX SPECTRA
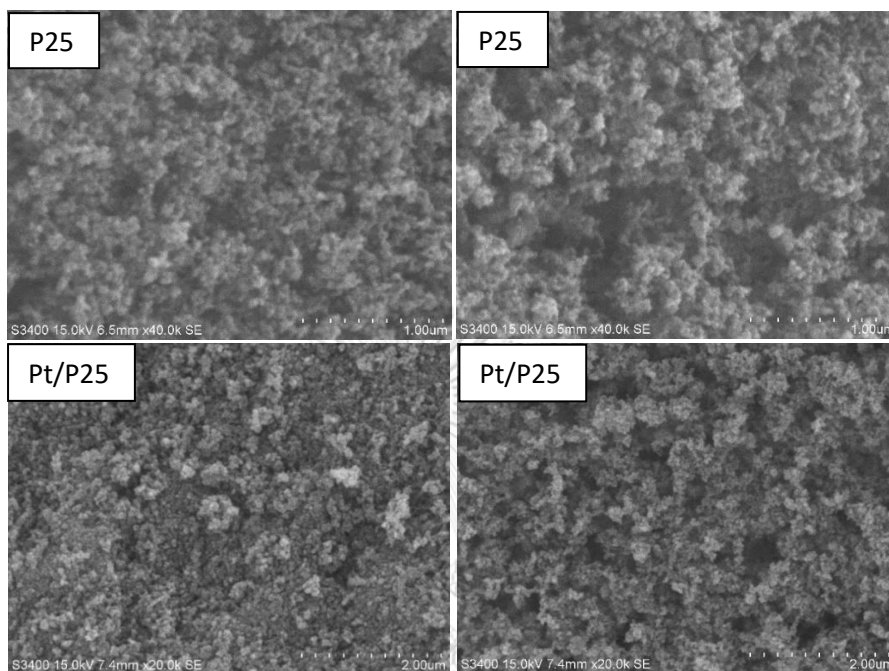

Figure 33 SEM images of pure P25-TiO$_2$ and Pt/P25 catalysts
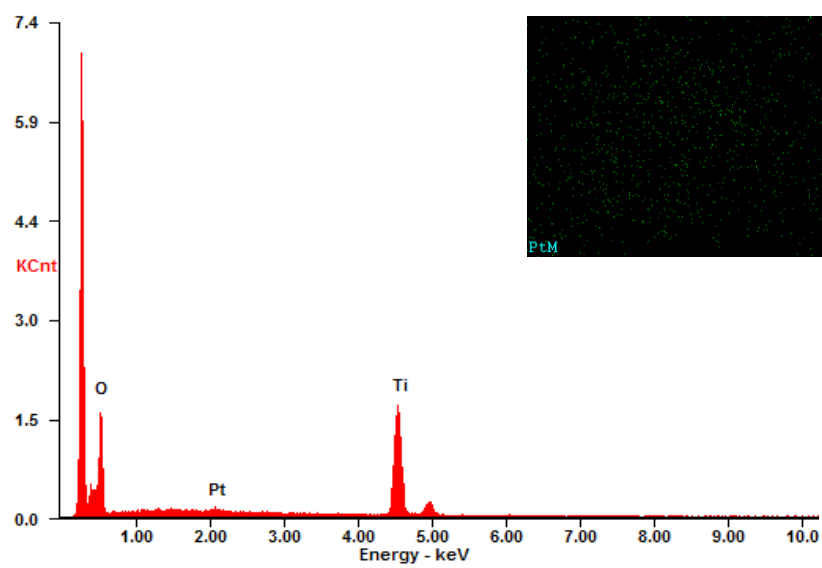

Figure 34 EDX spectra of Pt/P25 catalyst

APPENDIX G

CALCULATION OF PHOTOCATALYTIC PERFORMANCE

The quantitively photocatalytic performance was determined by using GC analysis. The calibration curve was used to calculate of reactant and product concentrations, as an example, the calibration curve of NB was shown in Figure 35.

Calculation of conversion of Ar-NO$_2$ and selectivity of Ar-NH$_2$ were defined as follow:

$$\%\text{Conversion} = \frac{\text{Mole (in) - Mole (out)}}{\text{Mole (in)}} \times 100$$

$$\%\text{Nitroaromatic conversion} = \frac{\text{Mole of nitroaromatic(in) - Mole of nitroaromatic(out)}}{\text{Mole of nitroaromatic (in)}} \times 100$$

$$\%\text{Selectivity} = \frac{\text{Mole of product}}{\text{Mole of consumed reactant}} \times 100$$

$$\%\text{Amino aromatic selectivity} = \frac{\text{Mole of desired amino aromatic}}{\text{Mole of consumed nitroaromatic}} \times 100$$
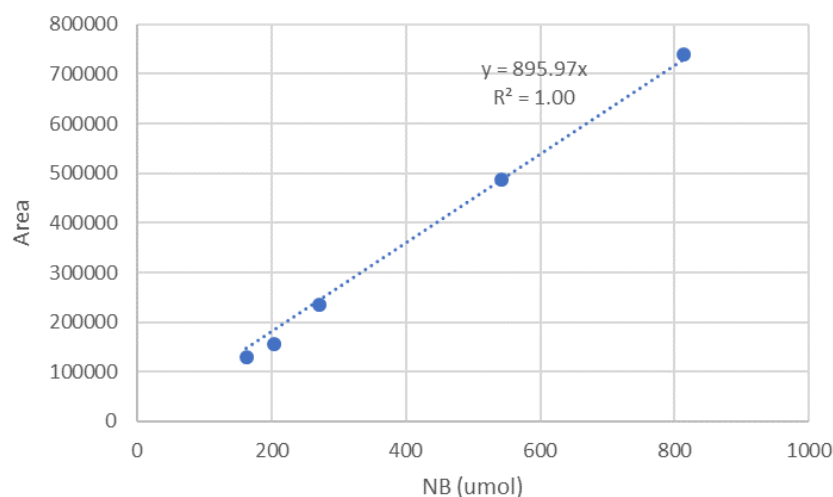

Figure 35 Calibration curve of nitrobenzene.

VITA

NAME	Pimchanok Nakchuai
DATE OF BIRTH	23 September 1994
PLACE OF BIRTH	Trang, Thailand
INSTITUTIONS ATTENDED	Bachelor of Chemical Engineering degree from King Mongkut's Institute of Technology Ladkrabang, Thailand in 2017 Master study in Chemical Engineering at Chulalongkorn University, Bangkok, Thailand in August 2017.
HOME ADDRESS	150/2 Village No.2, Banna Sub-district, Palian District, Trang, 92140, Thailand